POLITECNICO DI TORINO

Corso di Laurea in Ingegneria Biomedica

Tesi di Laurea Magistrale

Development of ultra-stretchable and conductive tactile sensor based on ionic liquids toward electronic skin

Relatori

PROF. Stassi Stefano

DOTT.SSA Chiappone Annalisa

Candidato

Ilenia D'Andrea

ANNO ACCADEMICO 2022-2023

ABSTRACT

In recent years, major technological advances in the robotics field have increased interest in the development of flexible pressure sensors capable of sensing mechanical stimuli. This can lead to significant changes, not only in biomedical applications, enhancing the treatment and care of patients with disabilities or amputations, but also in areas such as soft robotics and wearable devices, improving human-machine interaction. Here, a soft, conductive tactile sensor based on acrylate ionic liquid, cross-linked with an acrylate polymer and combined with polyimide copper electrodes is presented. Samples with different percentages of resin components have been obtained by photoreticulation process. The different formulations were studied and characterized by electromechanical tests to investigate the tensile and compressive stress sensitivity. The devices exhibit good mechanical properties (maximum elongation strain around 300%), as well as good electrical properties (gauge factor about 1.76) and stability when subjected to cyclic tensile tests with 100% strain. The applicability of this device was evaluated through detecting different signals of the human body. The results indicate that the developed sensors, based on acrylate ionic liquids, are potentially a good starting point for the realization of a stable, conductive, transparent, and low-cost electronic skin.

Table of Contents

List of figures

Chapter 1

Introduction

New technological advances in science, and specifically in robotics, have led to an increasing need for the development of an interface capable of connecting the human and robotic worlds.

These developments are needed to achieve significant changes in areas such as soft robotics and wearable devices, but particularly in the biomedical field, to achieve significant improvements in the production of devices that can improve the treatment and care of patients with severe skin damage or to integrate them into robotic prostheses to help patients who amputated a limb. For this reason, there has been growing interest in the development of flexible and conductive sensors that can detect stimuli from the outside world and thus achieve better human-machine interaction.

In this work, a transparent, soft and conductive tactile sensor based on ionic liquid that provides intrinsic electrical conduction and Poly(ethylene glycol) diacrylate that enables the creation of the 3D polymer network and stable structure is presented, all combined with polyimide copper electrodes to create the electrical connection between the sensor and the outside world.

Here, the entire process of manufacturing sensor was explored, starting with the choice of materials, and then moving on to its characterisation and applicability on the human body.
In particular, different formulations varying weight percentages of polymers were explored and characterized at a chemical and electromechanical level to investigate the sensitivity of the material to mechanical stress. In addition, it was also characterised at the biological level to assess its use in wearable applications.

Subsequently, the results obtained from the various characterisations were analysed and discussed. Based on these results, it is evident that the sensor is actually very stretchable, conductive, sensitive and cytocompatible.

Finally, in the last section, the performance of the sensor when applied to the human body was evaluated, showing the actual sensitivity to different signals such as bending at different angles and different frequencies of the finger, small deformations due to the hand flexor muscles, and finally the vibrational movements of the vocal cords.

The obtained results indicate that the developed sensor is potentially a good starting point for the realisation of an electronic skin that is flexible, easily adaptable to surfaces, conductive, transparent and with a low production cost.

Chapter 2

Flexible tactile sensors

In recent years, scientific research in the biomedical field has grown significantly as it aims to improve the lives of patients through the development of increasingly high-performance devices.

One of the main topics is the reproduction of sensory feedback to improve the perception-action cycle of patients with skin damage or limb amputation [1].

In particular, the skin is the largest organ in the human body, combining mechanical softness and sensory capabilities [1]. It represents the first protective barrier against external biological, chemical and physical agents. Moreover, it also has an important role in thermoregulation [2].

The sense of touch is located in the skin, which consists of three layers: the epidermis, dermis and subcutaneous tissue (*Figure 1*). The epidermis, forms the most external layer, composed of keratinocytes that produce keratin, which has a protective role. The dermis, the middle layer, consists of collagen, and lies on the last layer, the subcutaneous tissue formed by lipocytes[2].

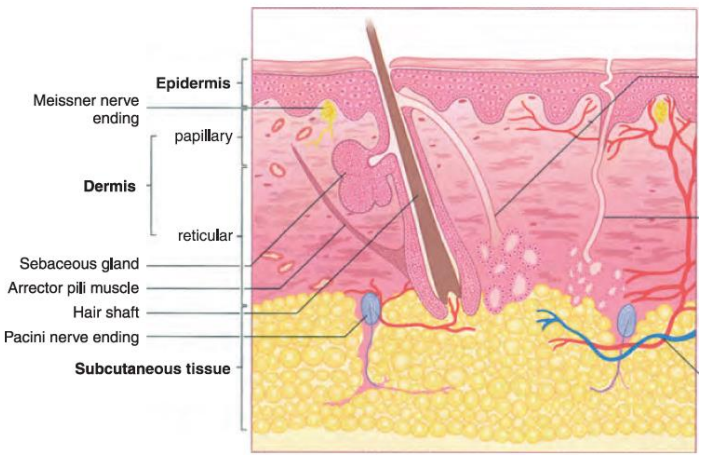

Figure 1 Scheme of human skin layers [2]

The transduction mechanism for the sense of touch is carried out by mechanoreceptors that interface with the nerve component and transmits the stimulus to the nervous system. Mechanoreceptors are located inside the skin and can be divided into two types, free nerve ending and low-threshold mechanoreceptors (LTMR). The former are capable of autonomous mechano-transduction, while the latter form corpuscles that act as receptors and are associated with specific neurons.

Somatosensory perception, information about the position and movement of our body is mainly attributed to the four tactile mechanoreceptors, Merkel cells, Ruffini endings, and Meissner and Pacinian corpuscles (*Figure 2*). Specifically, these mechanoreceptors are structures outside the axon and are associated with specific neurons that transmit the collected information to the central nervous system [3].

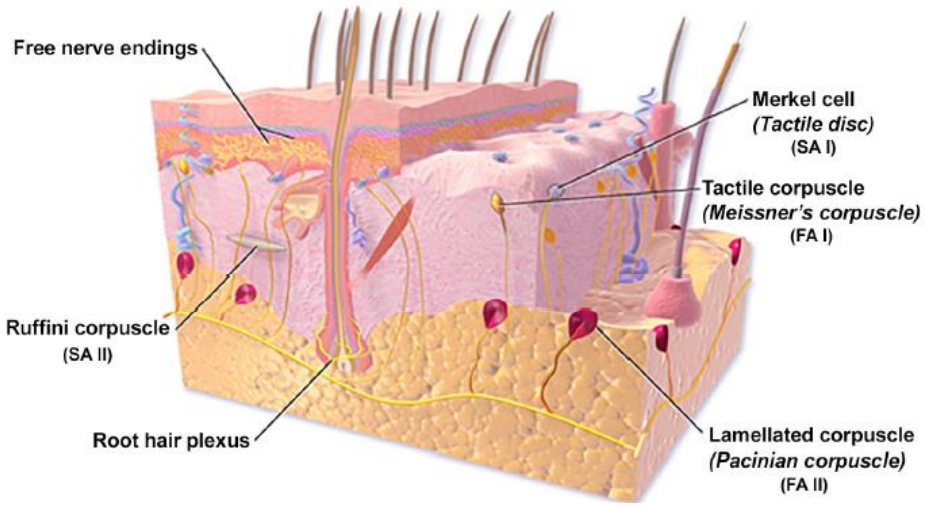

Figure 2 Tactile mechanoreceptors [3]

The corpuscles are distinguished according to the stimulus they are able to sense, specifically, Merkel cells are responsible for the uptake of pressure stimuli, Ruffini endings, on the other hand, are sensitive to skin stretching, while Meissner corpuscles are responsible for the uptake of skin rubbing stimuli, and finally, Pacinian corpuscles sense high-frequency tactile stimuli.

Nowadays, recreating this complex sensory system remains a major challenge, but much progress has been made in the sensing and differentiation of diverse stimuli. Strong technological advances in engineering have

contributed to the development of tactile sensors that can increasingly mimic the functions of human skin.

Sensors are devices capable of sensing external mechanical stimuli, such as pressure and strain, and converting them into electrical signals. This is made possible by the presence of a sensing element and a conversion element, specifically, the former corresponds to the part of the sensor that detects what is measured. Finally, the response to the stimulus is determined by several factors, such as the structure of the device and the characteristics of the material [4].

Recently, research is focusing more and more attention on ionic conduction mechanisms that better mimic the tactile transmission process, thus surpassing devices that relied on electronic conduction [5].

Analysing tactile sensation at the biological level, it can be noted that in a state of equilibrium, the ion channels present in human skin are closed, this allows the concentrations of cations and anions inside and outside the cell membrane to be controlled and kept constant [6]. When an external stimulus is applied, the ion channels on the cell membrane open and sodium ions present in the extracellular matrix flow into the cell, generating electrical signals (*Fig. 3*)[6].

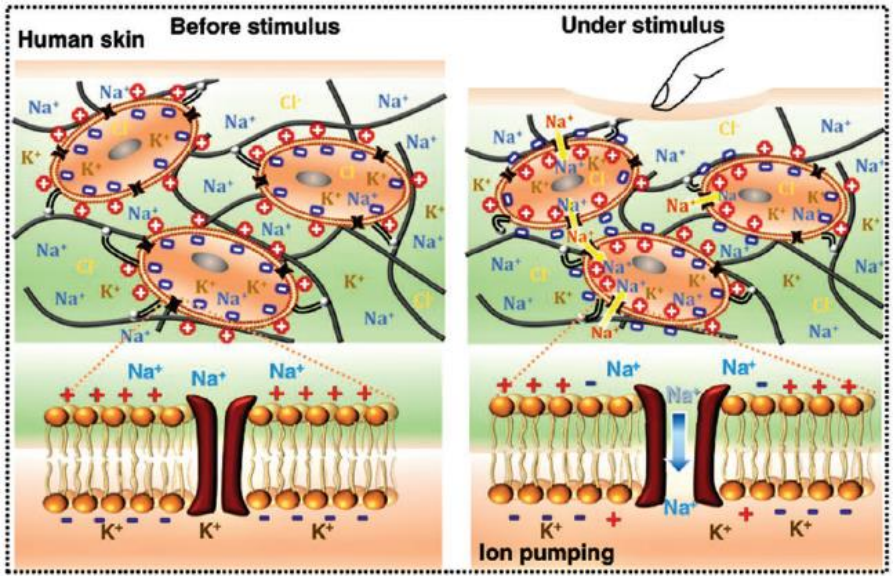

Figure 3 Scheme of the human transduction mechanism at the biological level [6]

Selecting the characteristics of the sensor is crucial and depends on the purpose of the device. In terms of mechanical properties, tactile sensors can be rigid, flexible, and especially durable as they acquire information through physical interaction and thus must be able to withstand impact and abrasion [7].

In addition, other fundamental parameters such as sensitivity, hysteresis, response time, sensing limit, durability, and mechanical stability must be considered for the development of pressure sensors. Sensitivity and hysteresis are fundamental parameters to be studied to evaluate the performance of the sensor produced. Sensitivity is important because it considers the structural changes, external and internal, that the sensor undergoes when subjected to a strain. Specifically, sensitivity is expressed as the ratio of the value of the electrical output signal to the variation of the applied input pressure or strain [4].

A sensor is considered to have good performance when it has high sensitivity values, thus, a small change in the input signal corresponds to a large change in the output signal.

Regarding hysteresis, it allows to describe the dependence of the sensor signal with respect to the mechanical loading and unloading history. In addition, the area enclosed in the hysteresis cycle corresponds to the work spent by the transducer to accomplish the full cycle. If the result corresponds to a straight line through the origin, it means that the element is perfectly elastic and therefore there is no energy loss (*Fig. 4*).

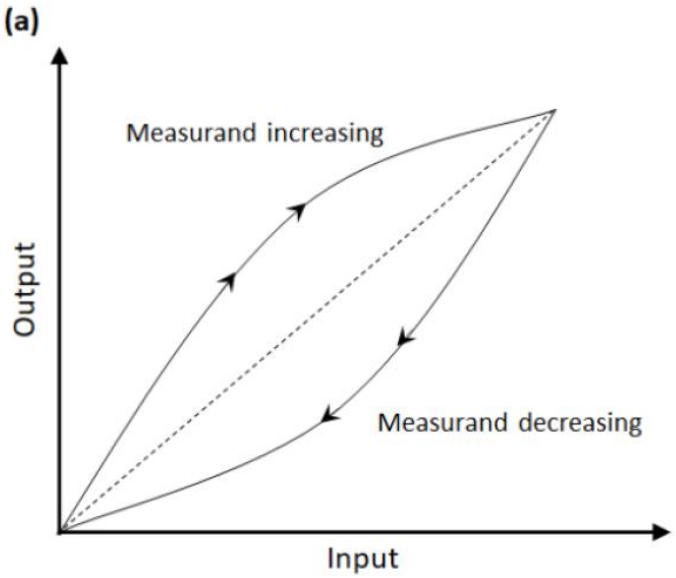

Figure 4 Representation of the hysteresis cycle

An important characteristic of human skin is to have a very large number of receptive nerve endings. This leads the skin to have very fast response times to stimuli and a good spatial resolution, being able to discriminate easily where the stimulus is applied. For this reason, response time and sensing limit are also two other important parameters to consider when developing a touch sensor.

The response time refers to how quickly the sensor responds to the application of an external stimulus, while the sensing limit corresponds to the minimum pressure that the sensor can detect [4].

Durability defines the performance of the sensor over time, verifying that it remains stable even when subjected to loading and unloading cycles. Lastly, in the evaluation of a sensor's performance, stability is another important parameter to consider and refers to the constancy of the sensor's performance over time, this is determined by several factors both chemical and physical.

2.1 Haptic sensor application

Over the years, technological advancement has been increasing and has enabled the development of materials and, consequently, sensory systems that perform better and more easily mimic the mechanisms of the world around us.

Initially, sensors based their working mechanisms on conventional electronics and the use of rigid materials. Subsequently, more and more flexible and easily stretchable materials were developed, which enabled the realisation of deformable electronic sensors. As mentioned earlier, the technological development that has taken place in these years has been enormous and has made it possible to go beyond conventional electronics and obtain the ability to mimic the potential generation mechanisms of human somatosensory receptors [8], realising tactile sensors capable of exploiting the high deformability of ionic conductors [8].

The realisation of this type of sensor allowed the creation of more high-performance wearable health sensors, in addition, it reduced the gap to the creation of an electronic skin and a better human-machine interface.

2.1.1 Electronic skin

The electronic skin (e-skin) mimics the human skin not only in terms of physical properties such as being thin, stretchable, soft and easily adaptable to the surface on which it is placed, but also in terms of the stimuli it is able to detect such as pressure stresses or temperature changes [4].

An example of this application has been published by Zhao et al., 2020 ,who have realised a device based on hybrid electrodes composed of p o l y (3, 4 - ethylenedioxythiophene):poly(styrenesulfonate)(PEDOT:PSS)/single-walled carbon nanotube (SWCNT) and enclosing a PDMS layer that acts as a dielectric layer (*Fig.5*) [9].

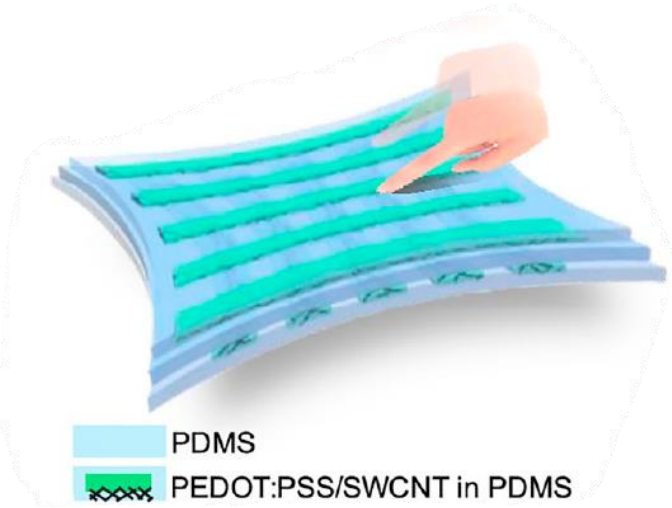

Figure 5 Example of the device realised by Cracco & al. [9]

Overall, the system is transparent and very flexible, and it can detect the applied pressure and the different states of deformation during stretching (*Fig.6*), due to the application of the conductivity conversion mechanism [9].

Figure 6 Representation of the different stretching operations applied to the device [9].

Finally, this sensor can achieve a deformation of 150%, good conductivity due to the presence of carbon nanotubes, and from *Figure 7*, it can be seen how well the device adheres to the skin [9].

Figure 7 Demonstration of good adhesion and adaptation of the device when placed on a non-linear surface [9]

2.1.2 Human-machine interfaces

Wearable electronics, characterised by high flexibility and excellent mechanical properties, are very important for the development of better human-machine interfaces [4]. These types of sensors can convert human movements into electrical signals [6], and in particular they must also be very robust to withstand abrasion, numerous washes and physical and chemical attacks from the external environment [4].

Xiao et al., propose a wearable device, capable of detecting movements and physiological signals even underwater [4]. This sensor is multilayered, starting with polyethylene terephthalate (PET) fibres from the inside, which, following a plasma treatment, are then coated with a network of carbon nanotubes (CNTs) and finally, as the last layer, a ppy-pdaperfluorodecyltrifluorotrioxysilane (PFDS) polymer is deposited to immobilise the CNTs and thus obtain a wearable and flexible sensor (*Fig.8*) [4].

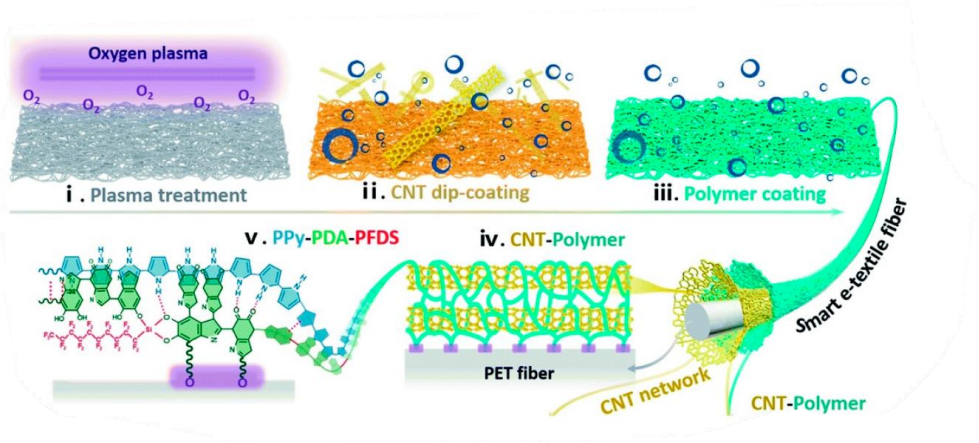

Figure 8 Schematic representation of the multilayer device[4]

Afterwards, the device was incorporated into a glove, and it was demonstrated how, through a signal acquisition and processing system, it could control a robotic hand through human hand movements [4]. *Figure 9* shows the application of the sensor to make the gesture of the word "I love you" [4].

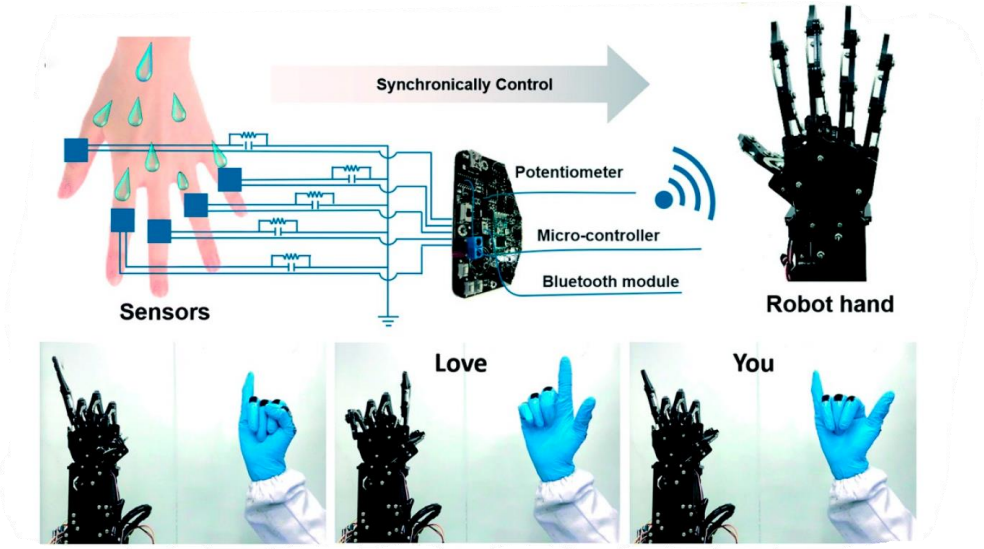

Figure 9 Representation of the functioning device that is able to synchronise the movement of the robotic hand through the movement of the human hand [4].

2.2 Transduction mechanisms

Haptic sensors can also be classified according to the transduction mechanism that determines the structural and material properties of the signal-sensing device, so it is possible to have piezoresistive, piezocapacitive, piezoionic, piezoelectric and triboelectric transducers.

Sensors that use piezoelectric effect have high sensitivity and resolution, but have the disadvantage of being expensive, complex to fabricate, and inflexible, so they are unsuitable for integration on a robotic body [7]. Whereas sensors that exploit the resistive and capacitive effect require the use of simple basic electronics and have low power consumption and manufacturing costs. They are also found to be more flexible and therefore easier to integrate. For this reason, these sensors are the most widely investigated [7].

2.2.1 Piezoresistance pressure sensors

Sensors using the piezoresistive effect considers changes in electrical resistance to determine strain when subjected to a mechanical stress. This effect is due to a significant change in resistivity under mechanical deformation that is strongly dependent on electron mobility and density[7].

Resistance, is therefore the quantity on which the piezoresistive transduction mechanism is based and can be expressed by *equation (1)*:

$$R = \rho\left(\frac{L}{A}\right) \quad (1)$$

where "ρ" is the resistivity, “A” is the cross-sectional area and “L” is the length [6].

These types of sensors are easily fabricated and involve relatively simple signal processing. Typically, they also exhibit low impedance and high sensitivity [5]. As can be seen in *Figure 10*, under the initial conditions, when no stimulus has yet been applied, the sensor is in a state of high resistance and the output current I_0 is relatively small. In contrast, the output current (I_P) increases after applying external pressure to the sensor under the same applied voltage [4].

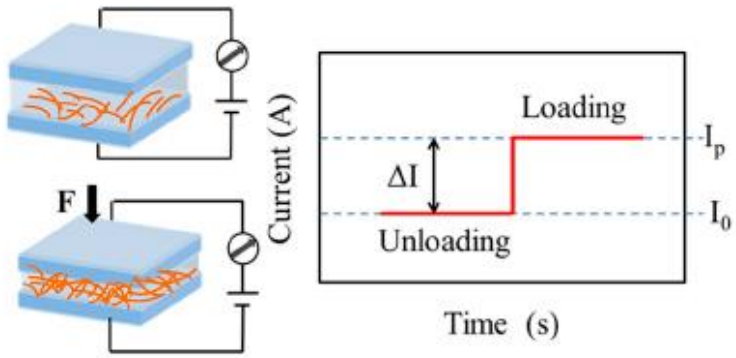

Figure 10 Working mechanism of a piezoresistive pressure sensor [4]

2.2.2 Piezocapacitive pressure sensors

Tactile pressure sensor that exploits the piezocapacitive effect are constituted by a capacitor, that consists of two electrodes separated by a dielectric material [10]. In particular, if the material between the two electrodes is soft, its deformation can lead to the change of sensing capacitance [10].

Specifically, the measurement of capacitance is expressed according to *equation* (2):

$$C = \varepsilon_0 \varepsilon_r \frac{A}{d} \quad (2)$$

where "C" is the capacitance, "ε_0" is the permittivity of the vacuum, "ε_r" is the relative permittivity, "A" is the contact area of the electrodes, and "d" is the distance between the electrodes [10].

In this case, there are two ways to achieve a change in capacitance in response to the application of a stimulus such as a pressure stimulus: vary the dielectric properties of the material, increasing the relative permittivity, or vary the geometry of the material, acting on the stiffness of the dielectric layer [10].

In particular, in order to induce geometric changes, for example reducing the distance between the two electrodes, one solution could be to decrease the value of the Young's modulus of the dielectric material in order to have a softer material that easily deform when subjected to external pressure. This consequently allows the sensitivity of piezocapacitive sensors to be improved [10].

These types of sensors have the advantage of low power consumption and fast response times [11]. In addition, they have low sensitivity because the dielectric materials used, such as elastomers or gels, have low dielectric constants, which induces lower reactivity when small pressure changes are applied [11].

Finally, *Figure 11* shows the structure of a capacitive sensor and how the signal pattern varies when an external pressure stimulus is applied. Initially, the capacitance value C_0 is low, and this is due to the distance between the two electrodes, later when the stimulus is applied and then the distance

between the plates is reduced, an increase in the final capacitance value C_p can be observed [4].

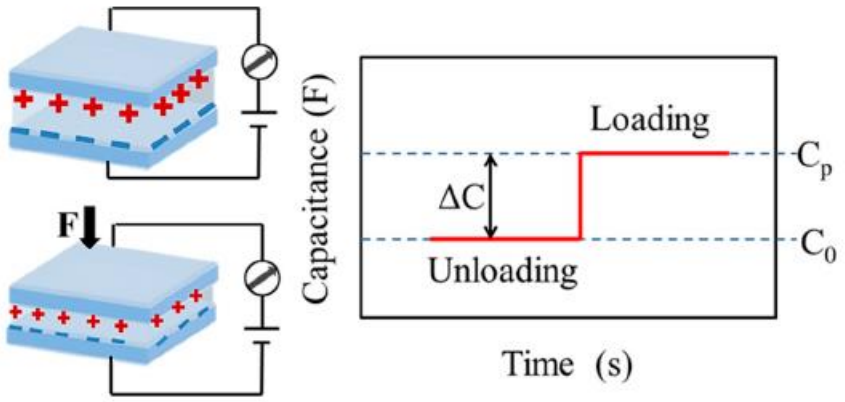

Figure 11 Working mechanism of a piezocapacitive pressure sensor [4]

2.2.3 Piezoelectric pressure sensors

Piezoelectric sensors have the peculiarity of using piezoelectric materials that can convert mechanical stresses applied on the device into electrical signals [6].

At the molecular level, following the application of an external stress, electrical charges accumulate at the ends of the material forming electrical dipoles, and it is the relative movement of anions and cations that generates the electrical potential [4].

Thus, the piezoelectric effect can be described as the dipole deflection that occurs in the material when a stress is applied, and it is the deformation of the crystalline structure of the material that causes the polarization [6].

In *Figure 12* we can see the working principle of these transducers.

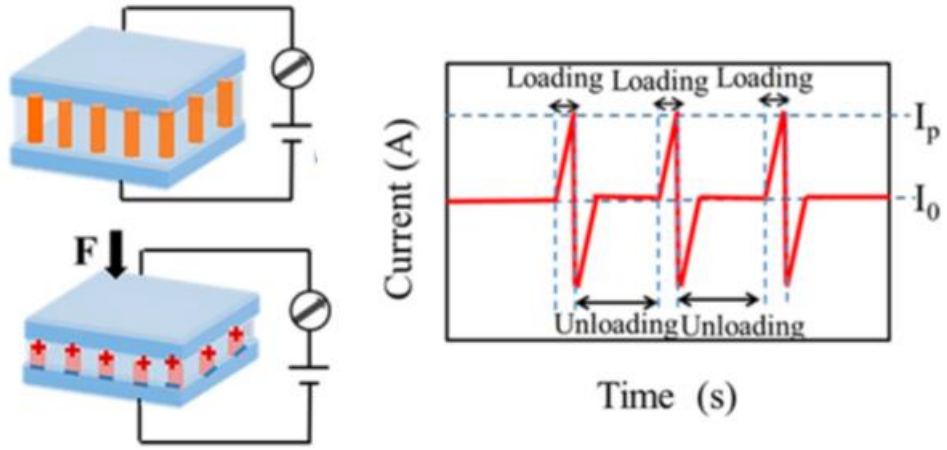

Figure 12 Working mechanism of a piezoelectric pressure sensor [4]

Another characteristic feature of piezoelectric sensors is that they are capable of self-powering without the aid of any external power supply, this has allowed them to be exploited in dynamic pressure sensing, but they have shown to have problems in detecting static pressure as they undergo signal attenuation and the output signal being susceptible to interference from the external environment [4].

To summarize, the major factor in these sensors is the change in polarization when an external force is applied to the sensor, and this can be caused by the reconstruction of the surrounding dipole or by the change in direction of the molecular momentum [5].

2.2.4 Triboelectric pressure sensors

Triboelectric sensors have the characteristic of being able to efficiently convert mechanical energy, generated by friction through the contact of different materials, into electrical energy [4]. Specifically, it is a type of contact electrification, where the mechanism of operation is described as the periodic formation of a potential difference between the charges on the inner surfaces in contact with each other, and at the moment the two surfaces are separated, an electric field is generated, and the device produces an output voltage [5].

The operating mechanism of these sensors is shown in *Figure 13* [4]

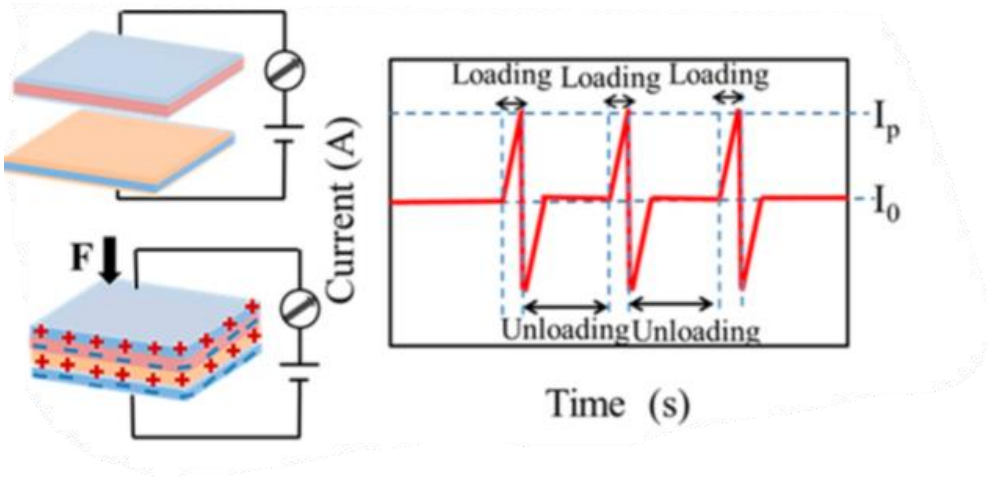

Figure 13 Working mechanism of a triboelectric pressure sensor [4]

These types of sensors, as well as piezoelectric sensors, are capable of self-powering and this feature makes them very effective in dynamic pressure sensing, however, even then static pressure sensing is still a problem due to charge recombination [4].

Triboelectric sensors were initially used as energy harvesting systems because of their high efficiency, low cost, low environmental impact, and the possibility of using them at low frequencies and later came to be used as tactile sensors as well [5].

2.2.5 Piezoionic pressure sensors

[12] defines the piezoionic effect as "*the transient separation of anionic and cationic species in a material (solvent-infused polymeric) in response to an applied mechanical stress, which can be measured as voltage or current"*[12].

The piezoionic effect is characterized by a working mechanism (*Fig. 14*) involving the application of an external mechanical stimulus that create a pressure gradient within the material and consequently leads to the formation of ion flux. Anions and cations have a different mobility that leads to their

separation over time, and it is the separation of these ions that produces a measurable ionic voltage and current [12].

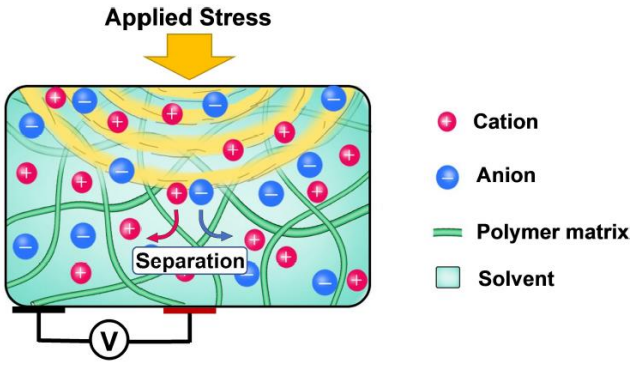

Figure 14 Working mechanism of the piezoionic effect [12]

Piezoionic sensors are made of flexible materials that are capable of self-powering and biocompatible, which makes them suitable for medical applications [13].

In addition, sensors characterized by the piezoionic effect have several advantages that make them an interesting object of study. First, mechanical transduction produces energy that enables both autonomous powering of sensing devices but at the same time can be exploited as an energy harvesting device [12]. Finally, this effect generates an ion-like output consequently integration with ionic biological processes is facilitated [12].

The fundamental limitation of this approach is the size of the ions, which are much larger than those of the electrons, and this leads to several consequences. For example, piezoionics turns out to be slower than electrons [12] consequently, sensors exploiting this effect require no more than a few tens of kHz [12]. The realization of devices that require being very small [12] is still difficult.

2.3 Ionic liquid

Ionic liquids (ILs) belong to a new family of organic materials, they consist of cations and anions (*Fig. 15*), which allows a very high number of possible combinations of ILs [13]. Specifically, cations are organic materials and can be classified as imidazole, pyridine, piperidine, amine, pyrrole, morpholine

and phosphine, whereas anions can be organic (salt of amino acids, sulphonated benzene, etc.) or inorganic (halides, tetrafluoroborate, hexafluorophosphate, etc.) [14].

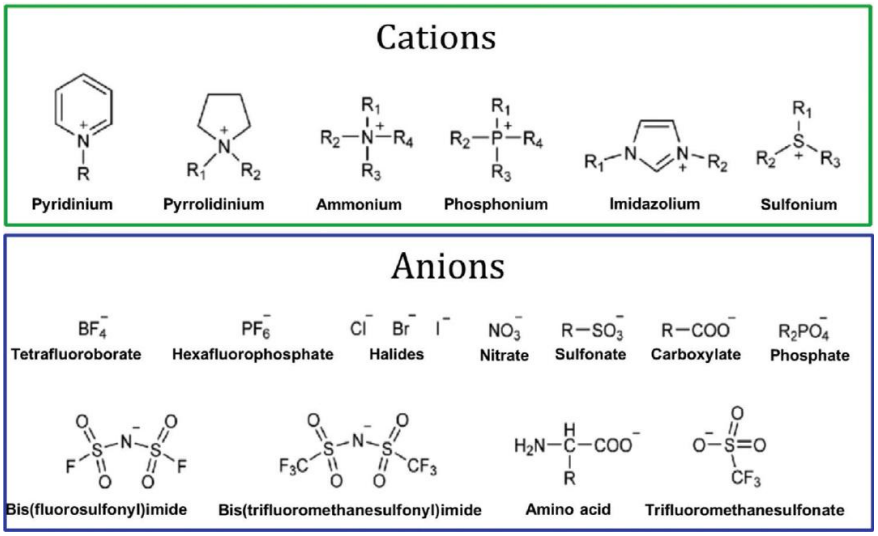

Figure 15 Some examples of anions and cations used to produce ionic liquids.[15]

However, it is important to note that the properties of ionic liquids are related not only to their structure but also to the interactions between the ions, in particular, coulombic, dispersion, H-bonds and van der Waals interactions [14]. Among these types of interactions, H-bonds are the most relevant as they determine the stability and miscibility of systems but also the hydrophilic and hydrophobic properties of ionic liquids [14]. Furthermore, it is interesting to note that the presence of water in contact with the system has a major impact on the H-bonds of the ionic liquids, because the anions of the ILs form new H-bonds with the water, breaking the H-bonds between the ion pairs in the initial ionic liquids [14]. In addition, ionic liquids have a low melting point below 100°C, which makes them ideal for use in biological applications. The main reason for this property is the non-stable structure due to the asymmetry and size of the ions, but also the delocalisation of charge and H-bonds [14].

From their studies of ionic liquids, [12] determined that these compounds exhibit important properties (*Fig. 16*) such as "*a low vapour pressure, a wide temperature window in the liquid state, high chemical and thermal stability, a wide electrochemical potential window, high ionic conductivity and good solubility in various organic or inorganic solvents*" [12]. Furthermore, recent developments have shown that they possess an ionic conductivity comparable

to many organic electrolytes, an extremely high boiling point up to 300°C, and an absence of decomposition with a broad electrochemical window up to 6 V [12].

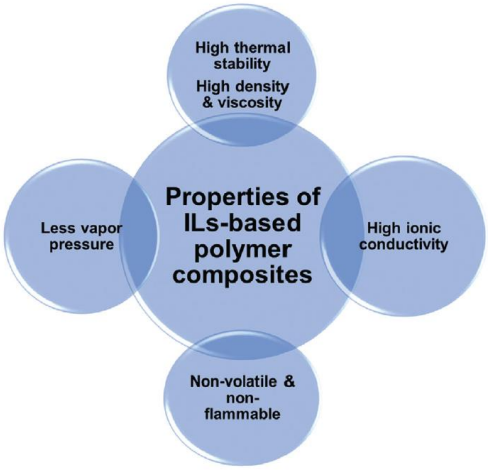

Figure 16 Major properties of Ionic Liquids based polymer composites [15]

Over the years, researchers are increasingly focusing their attention on the use of green and sustainable materials, and thanks to these properties, ionic liquids are increasingly being used in various research fields (*Fig. 17*) [15].

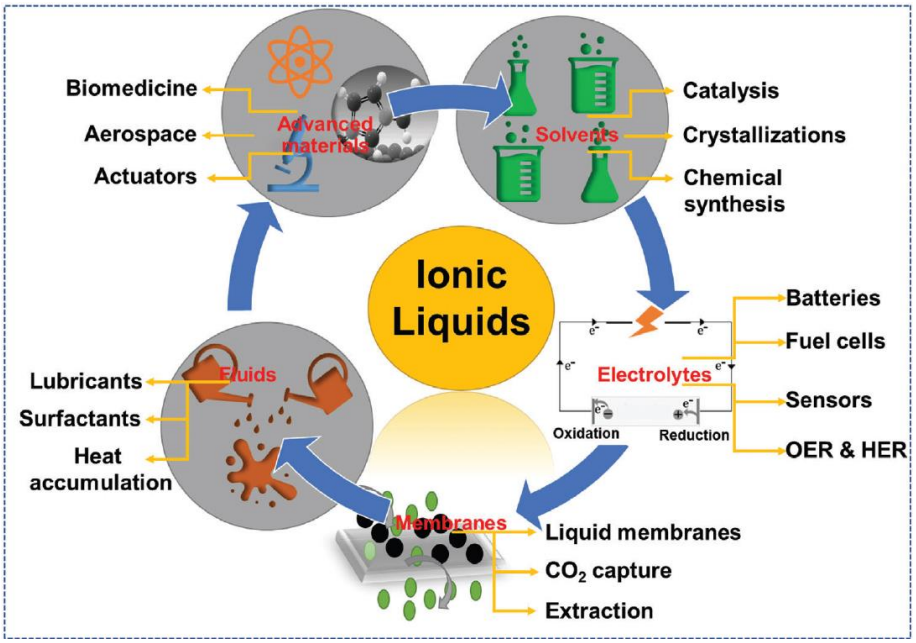

Figure 17 Several application areas involving ionic liquids [15].

For example, ionic liquids have been used to make sensors for glucose detection (*Fig.18*). In this case, the sensor is of the enzymatic type, in fact it

employs the enzymes HRP and glucose oxidase (GOD) in combination with a 3D microporous polymer (N[3-(trimethoxy silyl) propyl] aniline) based on ionic liquid ([BMIM][BF4]) [15]. The sensor was realised by immobilising the enzymes on the surface of the 3DMPTMSPA-IL composite polymer, using Nafion (Nf) as a ligand, thus creating the Nf-GOD-HRP/3DM-PTMSPA-IL/ITO biosensor, which performs very well due to its excellent selectivity and sensitivity, allowing it to detect a wide range of glucose concentrations [15].

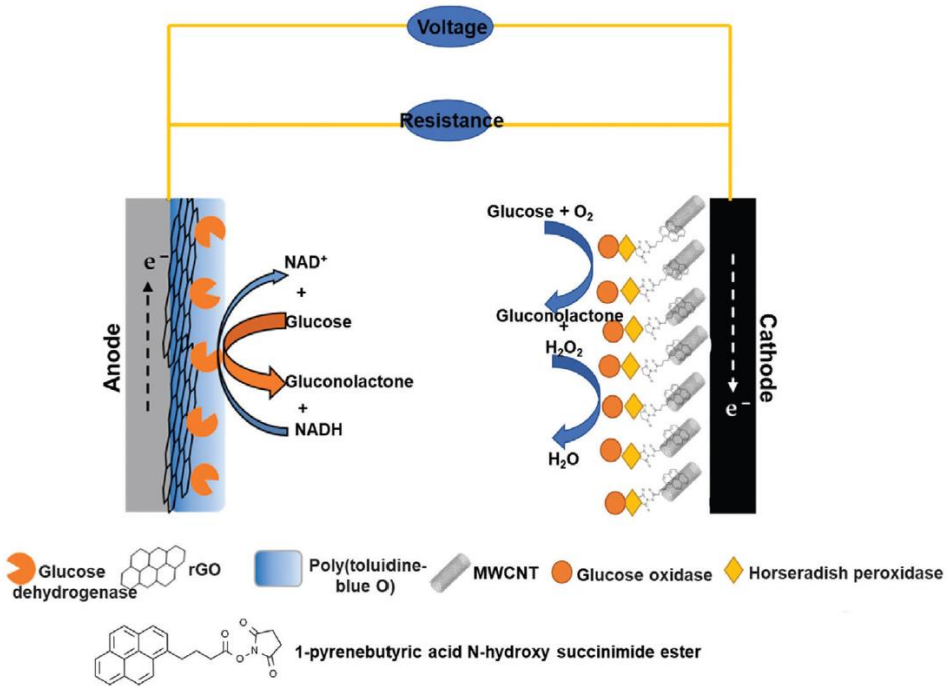

Figure 18 Representation of the glucose sensor designed on an enzyme bioassay cell [15].

Another example involves the use of ionic liquids in the field of energy. In this case, polymers combined with ionic liquids are used as electrolytes, and allow the formation of structures with ideal physico-chemical properties for energy management [15].

Supercapacitors (SC) defined by [15] as "*electrochemical devices that store and emit energy through an alternative process of adsorption and removal of ions at the interfaces of two electrode and electrolyte surfaces"* are an example of this application [15]. The operating mechanism of supercapacitors (*Fig. 19*) is the same as that of normal capacitors, differing only in the

material interposed between the two plates, which in this case corresponds to an electrolyte solution.

In this latter situation, it is ionic liquids that are used as electrolytes because they improve the energy storage performance of these devices, in fact they overcome many limitations imposed using previously organic or aqueous electrolytes [15].

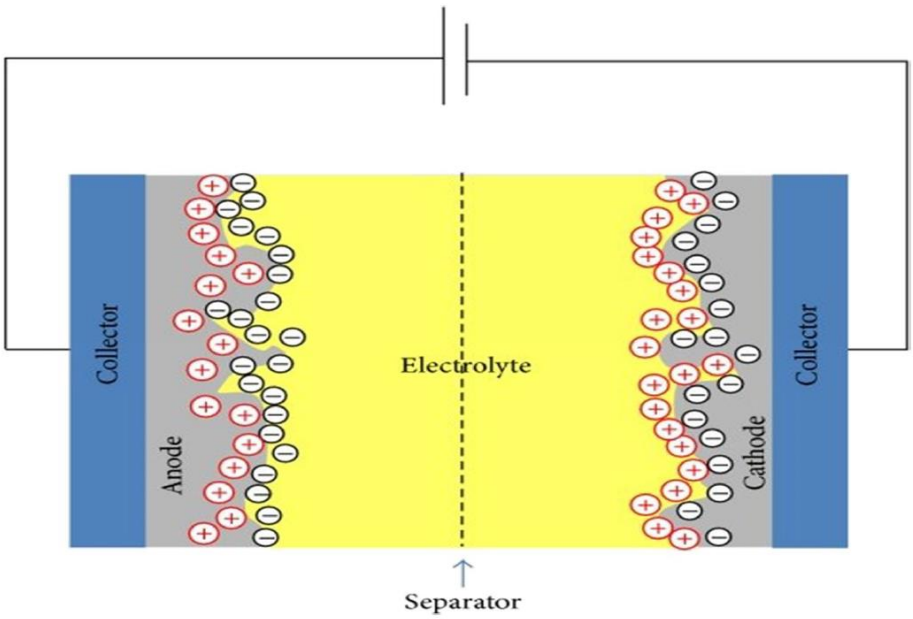

Figure 19 Representation of the working mechanism of supercapacitors [16].

2.3.1 Ionic liquid sensors

Therefore, ionic liquids considered in combination with other materials, such as polymers, are a potentially promising material for the realisation of touch sensors.

Indeed, there are several articles in literature dedicated to the development of tactile sensors based on ionic liquids.

For instance, Peng et al., 2022 present porous ionogel flexible sensors (PIFS) consisting of two monomers 2-hydroxyethyl acrylate (HEA) and 1,7,7-trimethylbicyclo(2.2. 1)hept-2-ylester,exo-2-propenoic acid (IBOA) cross-linked with poly(ethylene glycol) diacrylate (PEGDA700) to form a matrix

in which the ionic liquid 1-ethyl-3-methylimidazolium chloride ([EMIM]Cl) is dispersed (*Fig.20*).

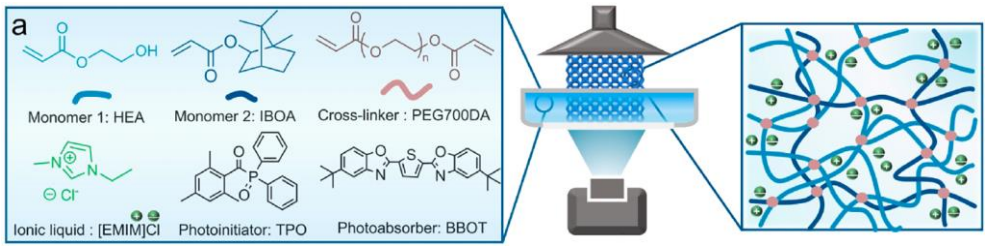

Figure 20 Representation of the compounds that constitute the IPFS and schematic drawing of the DLP 3D printer [17]

These type of sensors present a high sensitivity to pressure and a low hysteresis that allows stable signals to be obtained during dynamic loading tests, they also present an excellent environmental stability due to the non-volatile properties of the ionic liquids, but one of the most interesting results is that this material can be used with the Digital Light Processing (DLP) 3D printer, which allows systems with a high extensibility and a low Young's modulus to be obtained, and finally, and they were subsequently tested to monitor human movement (*Fig.21*) [17].

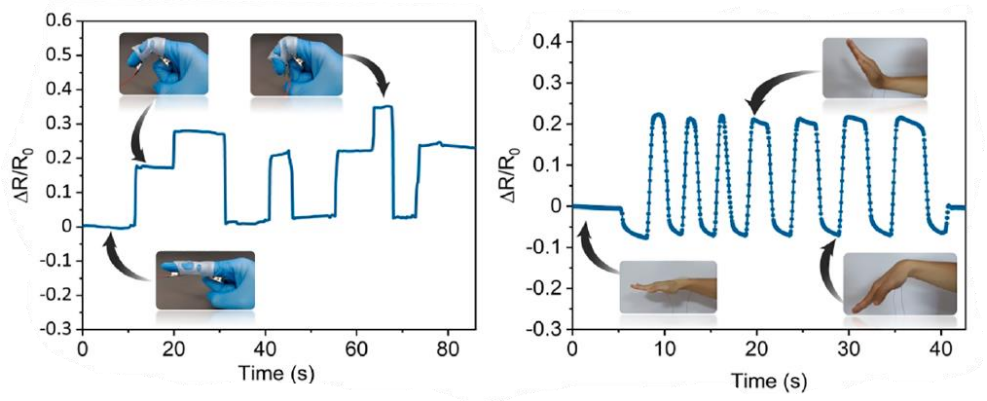

Figure 21 Diagram of tests performed to assess human movement [17].

Another example of a skin-inspired tactile sensor, based on ionic liquids, is presented by [18], which is realised by mixing thermoplastic polyurethane (TPU) with an ionic liquid (IL) 1-ethyl-3-methylimidazolium

bis(trifluoromethylsulfonyl)imide ([EMIM][NTf2]) and subsequently characterised (*Fig.22*).

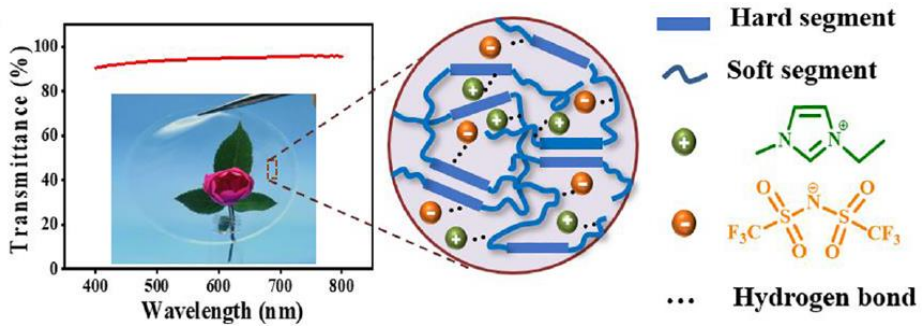

Figure 22 Representation of TPU@IL sensor composition [18]

The results show that these sensors exhibit high transparency, good strain sensitivity, accurate temperature perception and the most outstanding feature is good antibacterial activity followed by good cytocompatibility [18]. The antibacterial properties of the TPU@IL sensor, which was studied by using the zone of injection method, using Gram-negative Escherichia coli (E. coli) and Gram-positive Staphylococcus aureus (S. aureus) bacteria, which is evidenced by the formation of an "antibacterial ring" around the formulation [18]. From *Figure 23*, no ring formation occurs around pure polyurethane, on the contrary, as the ratio of TPU to IL increases, the ring diameter also increases. The enhanced antibacterial activity is due to the presence of the ionic liquid and in particular the cationic nature of the imidazole ring and the hydrophobic carbon chains that electrostatically interact with microbial cell membranes to lead them to cell death [18].

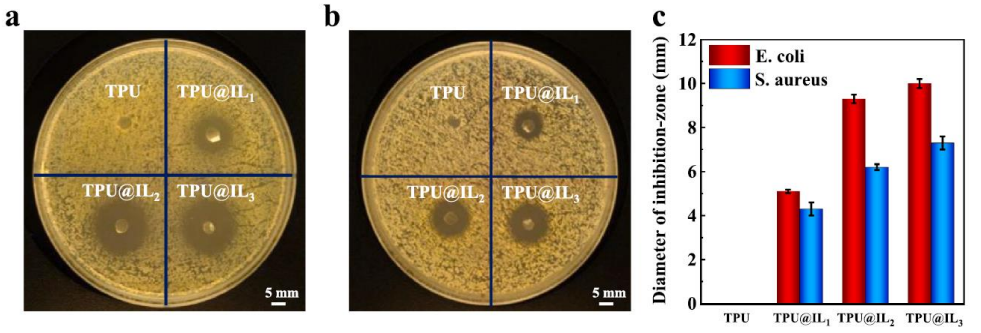

Figure 23 Visualisation of the antibacterial activity of the TPU@IL ionogel. a) E. coil bacteria, b) S. aureus bacteria. c) Diagram of the "antibacterial diameters" created in the inhibition zone when the system is exposed to E.coil and S.aureus [18].

Specifically, in *Figure 24*, on the left, can be seen the diagram representing the application of the TPU@IL ionogel as a strain sensor, highlighting the

relative change in electrical resistance over time as the wrist bending, while on the right, it can be seen the application as a temperature sensor in which the variation in temperature of a charging phone can be observed [18].

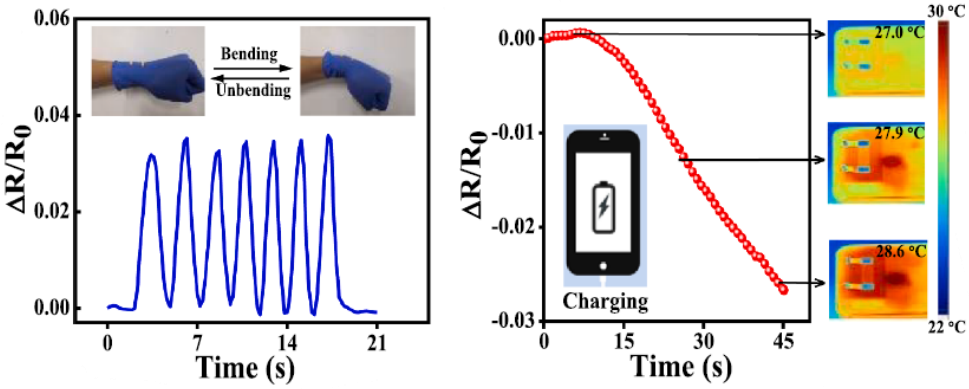

Figure 24 Applications of TPU@IL ionogel as strain sensor and temperature sensor [18].

Chapter 3

Materials and methods

In this thesis work, an ionic liquid-based tactile sensor was designed and characterised electrically and mechanically.

Figure 25 shows the sensor with a rectangular shape, which was made by mixing an acrylate ionic liquid, cross-linking it with an acrylate polymer and finally combining it with polyimide copper electrodes to measure electrical properties.

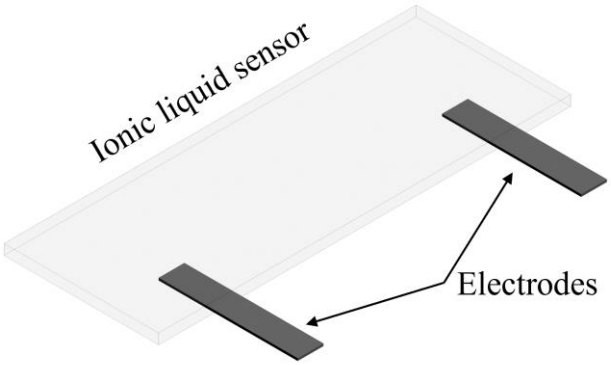

Figure 25 Final structure of the ionic liquid-based sensor

The sensor has characteristics such as transparency, which is useful in biomedical applications; flexible, adapting well to irregular surfaces; and lastly, soft, and conductive, in order to better mimic the characteristics of human skin.

In literature, there are a huge number of papers exploiting hydrogels and their properties to realise tactile sensors. Hydrogels are three-dimensional water-based polymeric systems and one of their possible disadvantages is that they are not very stable over time due to the evaporation of the aqueous part, which

causes the system to reduce its main characteristics of softness and, consequently, conductivity.

Moreover, conductive agents such as salt or metal nanomaterials or nanocarbons must be added to the hydrogels in order to make them conductive.

One solution to overcome the limitations of hydrogels was to create a material with a low water content, but still with highly conductive. For this reason, in this thesis work, the use of an ionic liquid as a matrix base for the realisation of a tactile sensor is investigated.

Therefore, the following materials were used:

- the ionic liquid [2-(Methacryloyloxy)ethyl]trimethylammonium chloride, used as the matrix base (*Fig. 26*). This ionic liquid is monofunctional, water-based and has the characteristic of being acrylate, which allows a strong molecular interaction between the chains and thus creates strong bonds without necessarily the presence of a crosslinker.

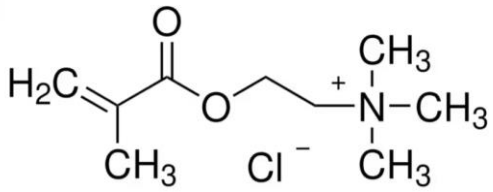

Figure 26 Chemical formula of the ionic liquid used in this work [https://www.sigmaaldrich.com/IT/it/product/aldrich/408107]

- Poly(ethylene glycol) diacrylate average Mn 700 (*Fig. 27*), is a bifunctional, biocompatible polymer used as a crosslinker to form the three-dimensional (3D) network due to the presence of acrylate groups [19]. The presence of this polymer improves the mechanical

properties of the material, in particular, it makes the final structure more stable.

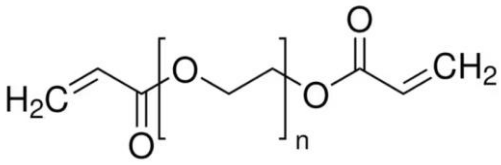

Figure 27 Chemical formula of PEGDA700 [https://www.sigmaaldrich.com/IT/it/product/aldrich/455008]

- the photoinitiator TPO-SDS, which has the particularity of being water-soluble. The photoinitiator is crucial in understanding the photocuring rate and, consequently, influences the final properties of the material and the time required for its manufacture [20]. Specifically, TPO-SDS was fabricated by mixing the synthesised lithium salt of 2,4,6-trimethylbenzoyldiphenylphosphine oxide (TPO) [20], a water-insoluble photoinitiator, with sodium dodecyl sulphate (SDS) in the percentages 10% TPO and 90% SDS, respectively.

Hence, *Figure 28* shows the process used to fabricate the sensor.

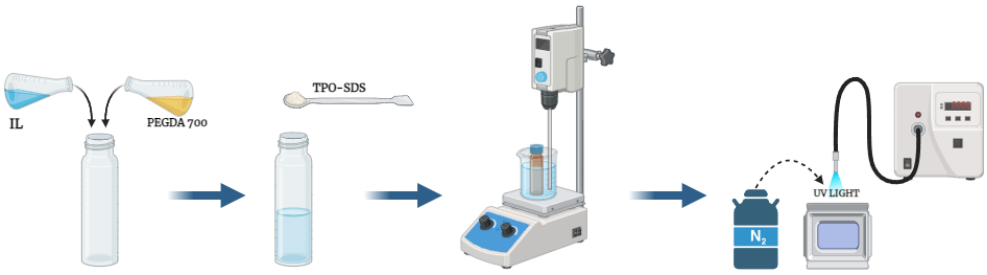

Figure 28 Representation of the chemical formulation preparation process

In particular, the ionic liquid was initially weighed and then 2wt% of PEGDA 700 and 1.5wt% of TPO-SDS were calculated based on the amount of LI inserted at the beginning and added to the formulation, taking care to cover the vial with aluminium foil to ensure that the formulation did not cross-link when exposed to light. Next, the formulation was heat-mixed with a magnetic stirrer at approximately 350rpp at 50°C for 15 minutes. In *Figure 29*, it can be seen that the formulation, after the preparation process, is transparent and well mixed.

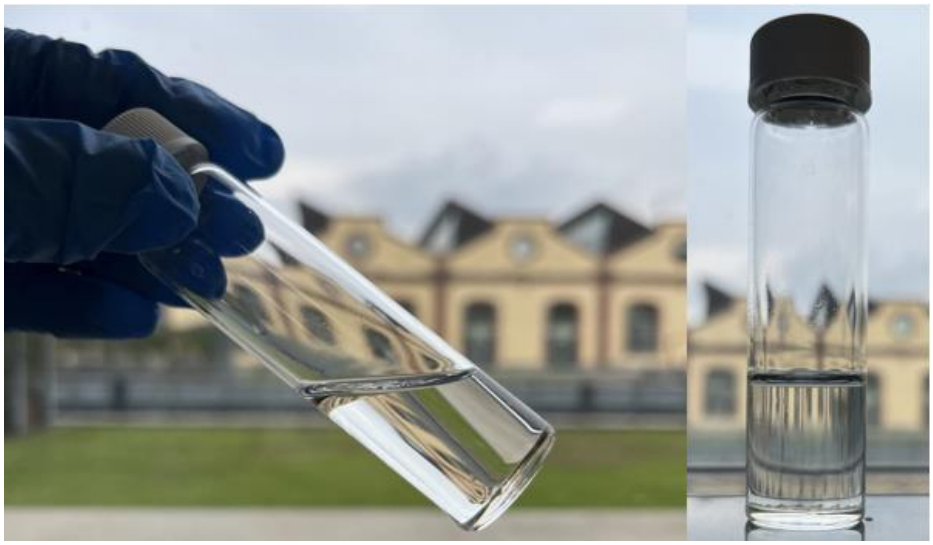

Figure 29 Formulation after mixing.

Subsequently, for sample preparation, the formulation was cast inside a rectangular Polydimethylsiloxane (PDMS) mould and exposed to UV light at a power of 200 W, at a pressure of 1 bar for 4.5 minutes per side while nitrogen is fluxed on the formulation.

Figure 30 shows the sensor realised following this manufacturing process.

Figure 30 Tactile sensor final result

3.1 Sensor Characterisation

Further to the preparation of the sensor, various experiments were carried out to study the material's chemical, mechanical and electrical characteristics. These methods will be discussed in more detail in the next sections.

3.1.1 Chemical characterisation

Rheology is a science that studies the behaviour of a material, be it liquid or semi-solid such as gels or polymers, when subjected to a deformation stress.

Through these tests, several parameters can be assessed, including viscosity, which evaluates the material's resistance to creep, and elastic modulus, which evaluates the material's stiffness, all of which define the characteristics of what is being analysed.

These properties, determined through the application of a shear stress, differentiate a wide range of materials that can vary from purely viscous to purely elastic, among these, materials that present intermediate characteristics are defined as viscoelastic.

In particular, the behaviour of elastic materials is described by the Hooke law (*Formula 3*), which represents the equation of a straight line:

$$\sigma = E \cdot \varepsilon \quad (3)$$

in which the deformation (ε) depends only on the applied stress (σ) and these two terms are related by the proportionality constant called 'Young modulus' or 'elastic modulus' (E) which provides information about the stiffness of the material and is identified by the slope of the line itself. In general, the response of elastic materials, independently of the intensity of the applied stress, follows a reversible linear trend, which means that all the mechanical energy supplied is absorbed and subsequently released when the stress ends, consequently, the material returns to its initial shape. Afterwards, the response begins to follow a non-linear and irreversible trend when a certain load defined as the 'yield point' is reached, and subsequently, by continuing to apply the stress it is possible to achieve the material's breaking point.

Whereas the behaviour of viscous materials is described by Newton law (*Formula 4*) which also represents the equation of a straight line:

$$\tau = \eta\dot{\gamma} \quad (4)$$

in which the shear rate ($\dot{\gamma}$) depends on the shear stress (τ) applied and these two terms are related by the proportionality constant called viscosity (η), which indicates the resistance opposed by the material to creep, which for this type of material can be considered as deformation. In particular, viscous materials present a linear and non-reversible response to applied stress, therefore all the mechanical energy supplied is not absorbed but it is lost in the form of heat and friction.

Finally, viscoelastic materials, which better represent reality, exhibit an intermediate behaviour between the two aforementioned. In particular, the deformation that is obtained following the application of a stress can be given by the sum of the elastic component and the viscous one. Therefore, the viscoelastic regime can be obtained when there is proportionality between the applied load and the deformation obtained, and this can be described with mathematical models obtained by combining Hooke equation and Newton equation.

In this work, the rheometer was used to evaluate the cross-linking time of the material studied through photoreological tests. The tests were carried out with an Anton Paar rheometer (Physica MCR 302) with parallel plates of which the upper one had a diameter of 25 mm, and a UV lamp (Hamamatsu LC8). The tests were conducted at a temperature of 25°C and imposing 200 micrometres between the plate and the glass plate on which the formulation was placed. Initially, the material was subjected to amplitude tests in order to search for the linear viscoelastic range (LVR), i.e. when the storage modulus (G') and loss modulus (G'') are stable. To achieve this condition, a constant oscillation frequency of 1 Hz was set and the amplitude of deformations was varied from 0.01% to 1000%. From the amplitude test, it was possible to choose an amplitude value (strain 2%) to be applied later.

Subsequently, photoreology tests were carried out at a constant frequency of 1 Hz and a strain value of 2% taken from the previous amplitude tests, this

allows the cross-linking time of the formulation to be assessed by looking at the variation of G' and G'' over time. The test starts by placing the formulation on the glass slide and then starting the mechanical actuation, after 60 seconds the UV lamp is switched on and kept on until the end of the test.

Therefore, these tests are useful for deriving the photoreactivity of the formulation and evaluating the use of the formulation for 3D printing applications.

Finally, the chemical characterisation of the material was performed by evaluating the insoluble fraction of the samples cross-linked with UV light according to the standard test method ASTM D276584 [21]. This test consists of measuring the weight of the sample, enclosed in a metallic net, before and after immersion in chloroform for 24 hours at room temperature. In particular, the chloroform allows the unreacted formulation to be removed. Subsequently, the sample was dried for a further 24 hours, to allow the chloroform to evaporate, and finally weighed again. The percentage of insoluble fraction was determined by calculating the weight difference before and after extraction of the sample from the solvent [21].

3.1.2 Electromechanical characterisation

In this study, various tests were carried out to characterise the material at an electromechanical level to determine the mechanical properties and sensitivity of the material when subjected to deformations, in particular, tensile break tests, cyclic tensile tests and compression tests were conducted.

To perform these tests, an Instron tensile machine associated with BlueHill software was used for the mechanical part, in which it is possible to set the parameters and acquire the mechanical data, while an LCR meter (BK Precision 894) associated with LabView software (National Instruments) was used for the electrical part (*Fig.31*), where it is possible to set the parameters and record the electrical data. At the end of the test, both data were elaborated using Matlab software and then analysed on Origin 2018.

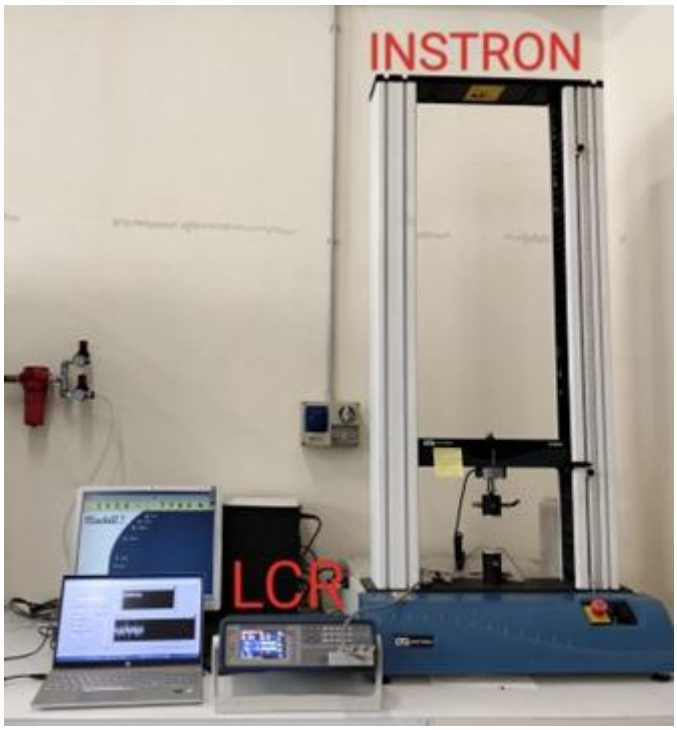

Figure 31 test bench for electromechanical tests

Several samples made with different weight percentages of PEGDA 700 (0wt%, 1wt%, 2wt% and 5wt%) were analysed. To carry out these first two tests, the sample size was measured, after which it was clamped between the grips of the tensile machine, together with kapton copper electrodes to which the LCR probes were attached. Then, the process parameters were set, the measurements being carried out, from an electrical point of view considering the parallel between a resistor and a capacitor as the impedance model, with a frequency of 1000 Hz and a voltage of 0,5V. From a mechanical point of view, a speed of 5 mm/min was set for the breaking tensile tests, while a speed of 10 mm/min and 100% strain was set for the cyclic tensile tests.

The tensile machine consists of two grips, one of which is fixed while the other is movable and moves thanks to the presence of a motor on which a load cell is mounted to measure the force applied to the sample by the machine. The actual stress felt by the sample is calculated using the *formula* (5)

$$\sigma = \frac{F}{A} \quad (5)$$

where F is the measured force and A is the cross-sectional area of the sample. On the other hand, the *formula* (6)

$$\epsilon = \frac{(l - l_0)}{l_0} \quad (6)$$

is used to calculate the strain, where l is the final length of the sample, and l_0 is the initial length of the sample, taking care to set the position to zero before the start of the test. Finally, these values allow the stress-strain curve to be constructed from which the mechanical properties of the specimen can be derived, and if the mechanical data are combined with the electrical one, the strain sensitivity of the specimen can be assessed.

Figure 32 shows the different phases of a tensile test in which the sample is stretched to failure.

Figure 32 Different phases of a tensile test in which the sample is stretched to failure.

Finally, the cyclic tensile tests present an identical setup to the tensile tests explained above and perform consecutive cycles of elongation and bending. In particular, for this test, the behaviour was evaluated at 20 cycles, at a speed of 10mm/min with 100% deformation.

Finally, compression tests were carried out using the LCR meter to detect electrical variations and the Instron tensile machine to detect mechanical variations with different grips in which the sample was sandwiched between two electrodes, resulting in a sandwich configuration. A preload of 0.05N was used to carry out these tests to establish the start of the measurement and a speed of 1mm/min, the test ended when a load of 50N was reached.

3.1.3 Measures of sample stability

During this work, the stability of the sensor over time was also evaluated using conductivity and durability tests.

The conductivity tests consisted of observing the change in conductivity over time, in particular, the measurement was conducted for 5 consecutive weeks and the sample was stored inside a petri dish at room temperature.

To evaluate electrical conductivity, an LCR meter (BK Precision 894) was used in conjunction with LabView software (National Instruments), and measurements were carried out at a frequency of 1000 Hz, a voltage of 0.5 V and imposing a signal acquisition duration of 30 seconds. To carry out this test, the sample was placed between two kapton copper electrodes connected to the LCR, as can be seen in *Figure 33*.

Figure 33 Set-up conductivity test over time.

The durability tests, on the other hand, consist of evaluating how the properties of the sample change when subjected to 50% deformation, also in this case the measurement was conducted under the same conditions as the conductivity tests.

To carry out this test, the Tensile Test Z5 machine was used in which the sample was clamped between the two grips together with the kapton copper electrodes, each of them connected to the LCR meter. Measurements were conducted at a speed of 10 mm/min and imposing a frequency of 1000 Hz, a voltage of 0.5 V.

3.1.4 Cytocompatibility tests

The sensor proposed in this work was tested for cytocompatibility in order to assess its applicability at the biological level in order to evaluate the use of the sensor for wearable applications.

These tests were conducted on HaCaT cells (human keratinocytes) using the Metabolic Activity Assay (MTT) or 3-(4,5-dimethylthiazol-2-yl)-2,5-diphenyltetrazolium bromide assay, that is a colorimetric assay for assessing cell viability and proliferation and it is conducted at 24 hours and 72 hours. MTT is a yellow tetrazolium salt that is reduced by live cells to a purple/blue formazan product.

Different formulations were tested by varying the type of photoinitiator used. In particular, the standard formulation with TPO-SDS and another with Lithium phenyl-2,4,6-trimethylbenzoylphosphinate (LAP), a cytocompatible photoinitiator with similar properties to TPO-SDS, were studied.

Initially, the samples were subjected to several washes with a solvent, ethanol, to remove unreacted components, followed by further washes with aqueous solution to remove the ethanol.

To increase the chances of cell survival, four different combinations of washes were evaluated:

- 20 minutes sonication in ethanol + overnight in PBS
- 20 minutes sonication in ethanol + 10 minutes sonication in PBS
- overnight in ethanol + overnight in PBS
- overnight in ethanol + 10 minutes sonication in PBS

After the washes (*Fig.34*), the samples were further sterilised by exposing them to UV light 30 minutes per side in order to remove other potentially cell-damaging substances.

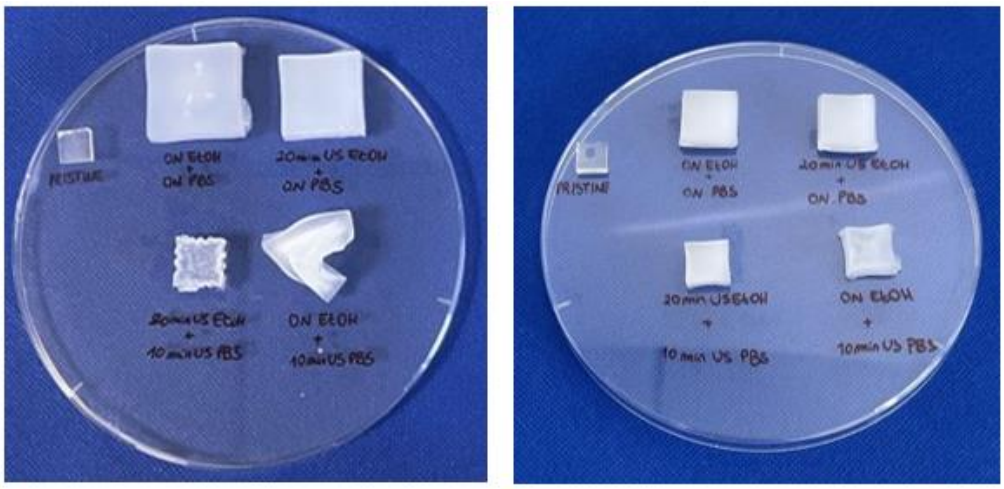

Figure 34 Representation of the samples after washing. Left, the samples made with the TPO-SDS photoinitiator. Right, samples made with the LAP photoinitiator.

Subsequently, the samples were incubated (*Fig.35*) in 10 ml of culture medium (DMEM + GlutaMAX-I) for 2 days, thus obtaining the conditioned medium that will be used in the MTT.

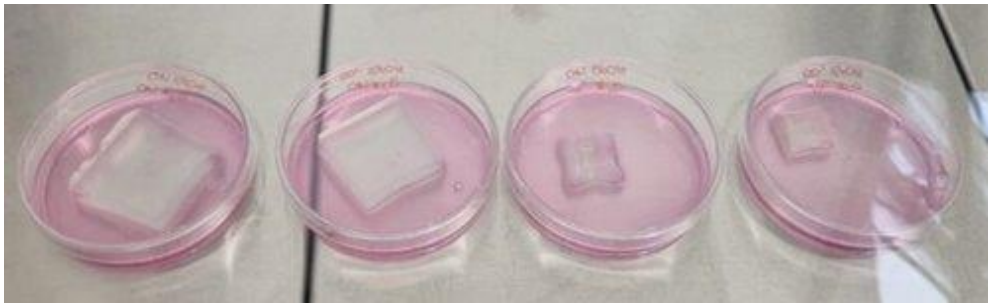

Figure 35 Immersion of sterile samples in culture medium

Meanwhile, HaCaT cells (human keratinocytes) are cultured in DMEM (gibco) supplemented with 15% FBS, 2% L-glutamine, 1% penicillin-streptomycin and 1% sodium pyruvate. Before the experiment, the HaCaTs are detached with trypsin (0.25%).

The HaCaT are seeded at a concentration of 10 000 cells/well in a 96-well plate and the various conditioned media are added.

After 24 or 72 hours, 200 µl of MTT reagent is added directly to the cell culture medium. The MTT is taken up by the cells through endocytosis. Within the cell, MTT is converted into formazan, this reaction depending on the metabolic activity of the cells.

After incubation with MTT, the medium is removed and the cells are lysed to solubilise the formazan crystals, using 200 µl of DMSO.

The absorbance of the solubilised formazine is then measured with the UV-vis spectrometer at a wavelength of 570 nm, in particular, the absorbance is directly proportional to the viability of the cells.

Chapter 4

Results

4.1 Photoreology

The sensor was chemically evaluated by time sweep tests at constant frequency and amplitude, considering values of 1Hz and 2% respectively. Specifically, the amplitude value was determined by looking at the region of linear viscoelasticity (LVE) in which the formulation is stable, obtained by performing an amplitude sweep test on the liquid formulation (*Fig. 36*).

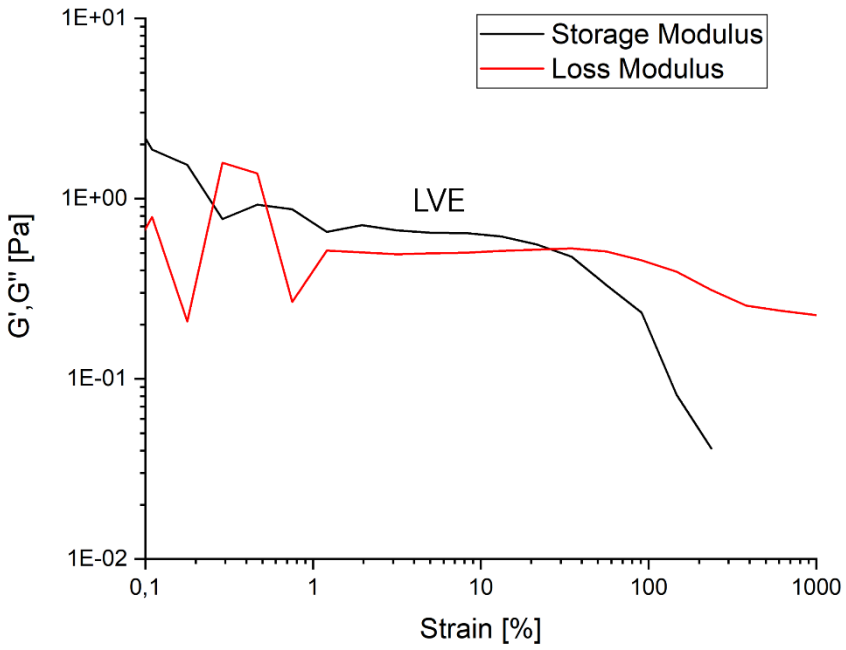

Figure 36 Amplitude sweep test result showing the linear viscoelasticity region.

Time sweep tests allow us to assess the reactivity of the formulation when exposed to UV light.

According to the results obtained (*Fig. 37*), it can be seen that all formulations, including the control, are very reactive.

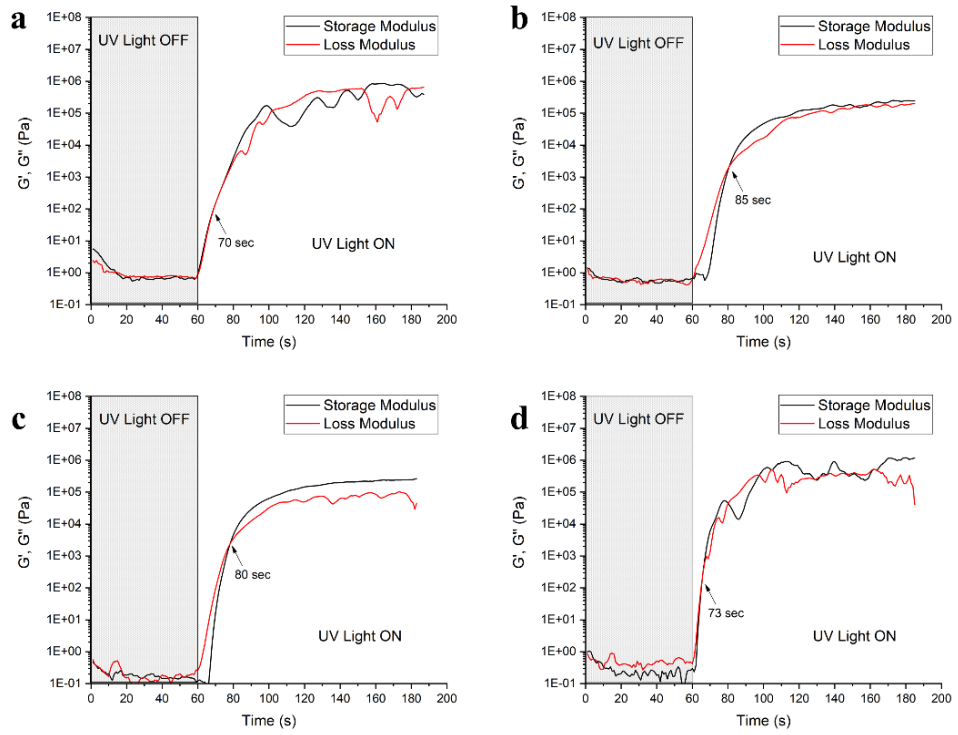

Figure 37 Time sweep test results. ***a)*** *Results trend of the control formulation* ***b)*** *Results trend of the formulation with 1wt% PEGDA 700* ***c)*** *Results trend of the formulation with 2wt% PEGDA 700* ***d)*** *Results trend of the formulation with 5wt% PEGDA 700*

Regarding the control (*Fig. 37a*), it is not possible to exactly define the gel point as the curves overlap from the beginning. Anyway, observing the trend of G', it is possible to see that G' starts to rise immediately but has a lower slope than the other formulations. In this case, there is the formation of a non-cross-linked polymer, in which the monomer has undergone an increase in molecular weight with the possible formation of strong intramolecular attraction bonds due to the charges, which means that the instrument actually detects the formation of a more rigid structure whose properties, however, increase more slowly.

Instead, in the case of samples with different concentrations of PEGDA 700 (*Fig. 37b, c, d*), it can be seen that when the UV light is switched on, there is a slight delay at the start of growth, but once this has been overcome, the curve acquires a much steeper trend with the subsequent formation of the cross-linked material. In addition, with the addition of PEGDA700, it is possible to observe that there is a reduction in the gel point and an increase in

the slope of the curve as the amount of crosslinker increases, this effect is due to the fact that a more crosslinked structure is created.

4.2 %GEL

The %GEL test (standard test method ASTM D276584) was performed to evaluate the actual crosslinking of the material, this information can be useful to assess the stability of the material. In *Table 1* it can be seen that the percentage variation of the sample weight is less than 10%, this means that the sample is well crosslinked and only a small part of the formulation did not react.

%GEL in CLOROFORMIO	Peso Campione (mg)	Peso Retina (mg)	Peso Retina + Campione (mg) (**PRIMA** del %GEL)	Peso Retina + Campione (mg) (**DOPO** del %GEL)	Variazione Percentuale (%)
S1	182,7	785	965,5	955,7	6,6%
S2	164,8	1210,4	1373,2	1363,3	7,2%
S3	201,6	814,2	1014,5	1002,9	6,4%

Table 1 Results of the %GEL test

4.3 Tensile tests

In the tensile tests, the sample was stretched up to breaking point.

In order to assess the mechanical performance of the sample, stress-strain curves were constructed in which it is possible to see how much the sample is able to deform depending on the stress applied. From the graph in *Figure 38*, it can be seen that the control sample is itself very elastic, in fact it reaches a deformation of around 300%, while looking at the samples with the different weight percentages of PEGDA, it is possible to see a decreasing trend in the elongation of the sample as the concentration of the crosslinker increases.

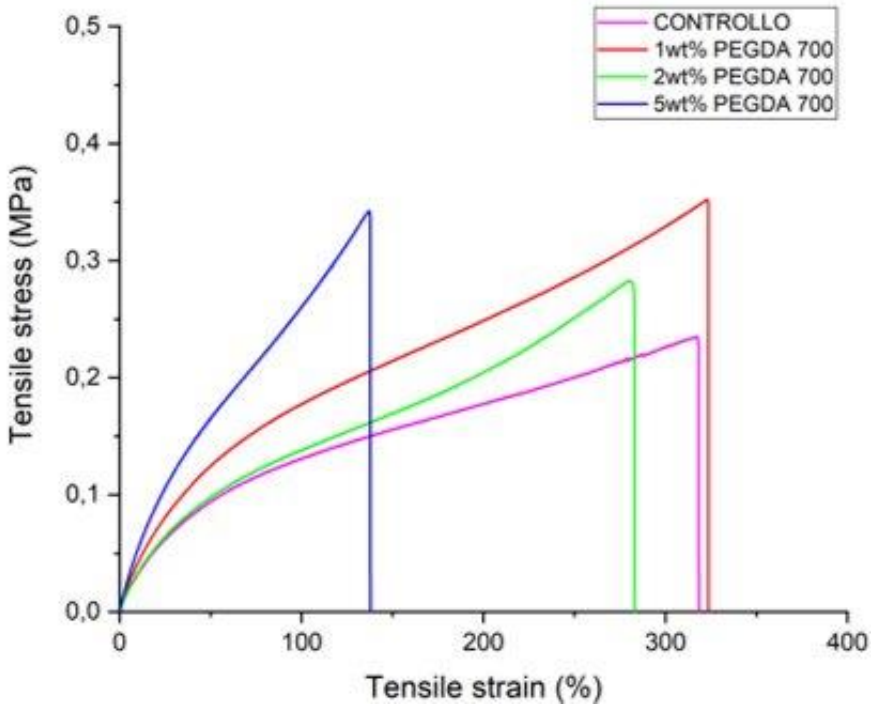

Figure 38 Stress-strain curves of control and formulations with different weight percentages of PEGDA700 compared.

Figure 39 shows the bar graph of the change in Young modulus. From the data it appears that with low percentages of PEGDA700, the elastic modulus remains fairly unchanged, on the contrary, in the formulation containing 5wt% of PEGDA700 it can be seen that there is an increase in G'. This is due to the fact that a greater number of bonds are created making the polymer more rigid.

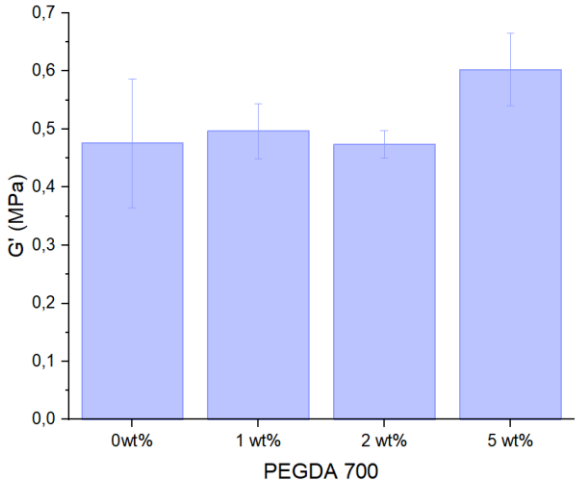

Figure 39 Bar chart of Young Module of control and formulations with different weight percentages of PEGDA700 compared.

In order to evaluate the electrical behaviour of the sample, curves were constructed in which the percentage change in resistance is related to the mechanical deformation (*Fig.40*), and it was then possible to determine the sensitivity value of the sensor by evaluating the slope of the curves in three different zones: "beginning" (0%-35%), "middle" (100%-135%), "end" (200%-235%).

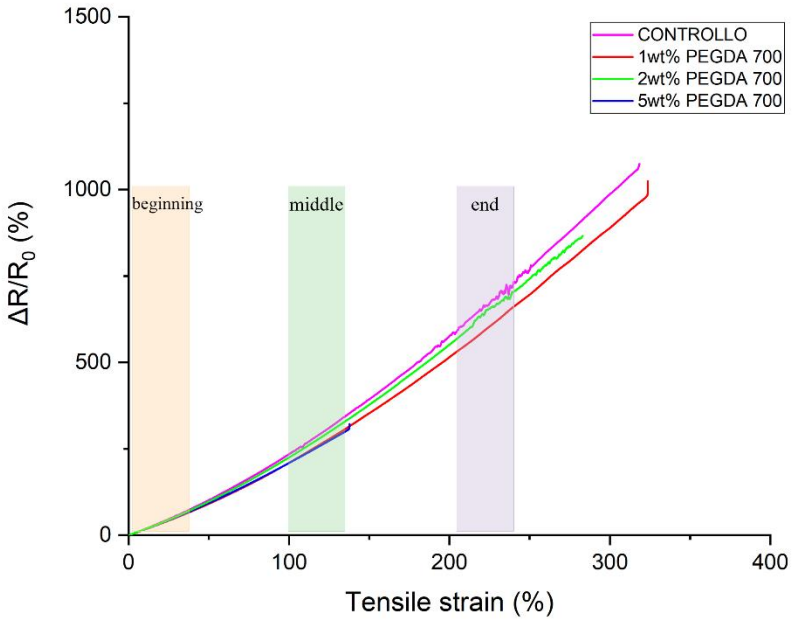

Figure 40 Graph for sensitivity calculation. The ranges 'beginning', 'middle' and 'end' indicate the sections of the curve from which the slope values were extrapolated.

In the graph in *Figure 41*, the statistical analysis of the sensitivity shown that control sample and those with 1wt% and 2wt% of PEGDA 700 are similar, whereas there is a decrease in sensitivity in the sample with 5wt% of PEGDA 700.

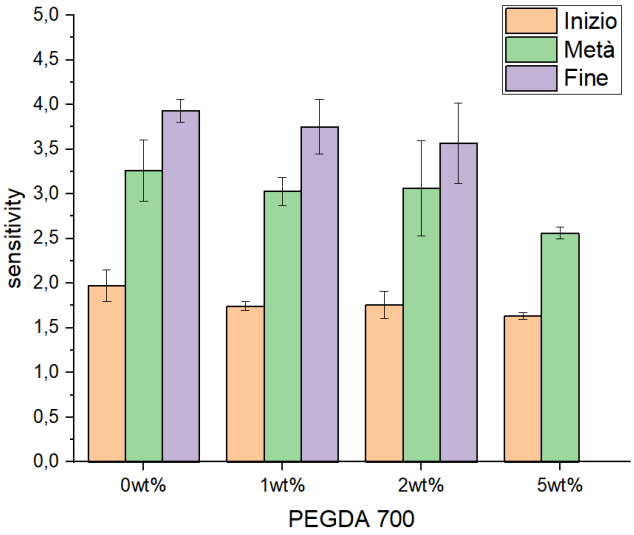

Figure 41 Statistical analysis of the sensitivity

The samples were also tested as force sensors (*Fig. 42*), and it is interesting to note that the performance of the control and that of the sample with 2wt% PEGDA700 are very similar in the range between (0 - 0.2 MPa), which means that the sample cross-linked with 2wt% PEGDA700 can detect changes in strength even with small stresses.

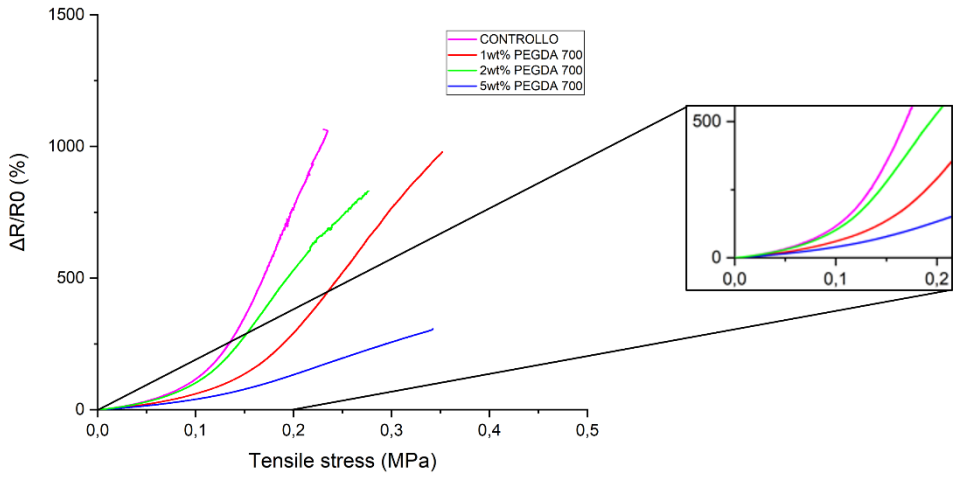

Figure 42 representation of the behaviour of samples evaluated as force sensors.

Afterwards, further tests were carried out to determine which formulation had better electromechanical properties. In the cyclic tensile tests, the specimen was subjected to 20 loading and unloading cycles to 100% deformation.

On the mechanical side, from the stress-strain curves (*Fig. 43*) of the control sample (Fig. 43a) it can be seen to have a viscoelastic behaviour that leads it to have a particular hysteresis cycle that differs from the samples containing the cross-linking agent. For formulations with PEGDA700 (*Fig. 43 b, c, d*), on the other hand, the sample is more stable and therefore less viscoelastic, which makes it more reproducible over time, so the sample when subjected to further deformation cycles is capable of maintaining the same mechanical properties.

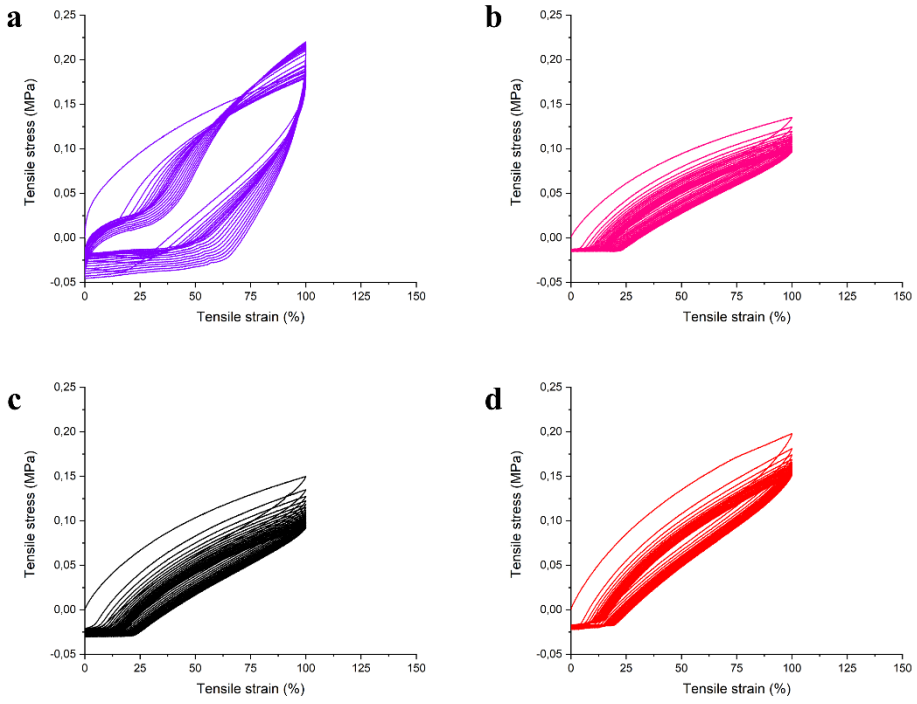

Figure 43 Representation of stress-strain curves of cyclic tests. ***a)*** *control formulation with 0wt%PEGDA700* ***b)*** *formulation with 1wt%PEGDA700* ***c)*** *formulation with 2wt%PEGDA700* ***d)*** *formulation with 5wt%PEGDA700*

Also from an electrical point of view, when looking at the percentage variation in resistance in relation to time (*Fig. 44*), the viscoelastic behaviour of the material identified by the drift of the curve is clearly visible in the control formulation, while in the samples with the PEGDA700, the percentage variation in resistance is more stable and similar in amplitude, so there are few variations and the behaviour of the sample with the PEGDA700 is poorly viscoelastic, therefore in this regard we can also confirm that the samples are more repeatable.

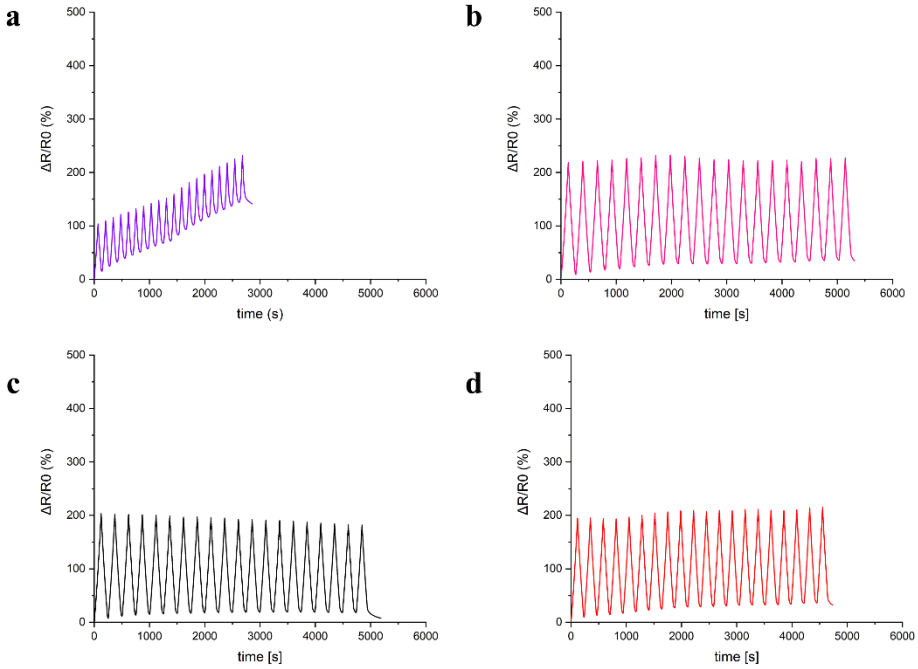

Figure 44 Representation of change in electrical resistance over time of cyclic tests ***a)*** *control formulation with 0wt%PEGDA700* ***b)*** *formulation with 1wt%PEGDA700* ***c)*** *formulation with 2wt%PEGDA700* ***d)*** *formulation with 5wt%PEGDA700*

Based on the observation of the results of the tensile tests at break and cyclic tensile tests, it was determined that the formulation containing 2wt% PEGDA700 was the best compromise, both in terms of elongation, reaching more than double its initial length, and for its low viscoelastic behaviour with the most stable variation of electrical resistance over time compared to the other formulations, which is why subsequent tests were only conducted on samples with this formulation.

4.4 Stability tests

Stability tests were carried out to assess the consistency of electrical and mechanical properties over time.

From the results of the conductivity tests carried out for five consecutive weeks, observing the statistical analysis (*Fig. 45*), it is possible to see how the conductivity value decreases over time and this behaviour may be due to the evaporation of the small part of water present within the ionic liquid.

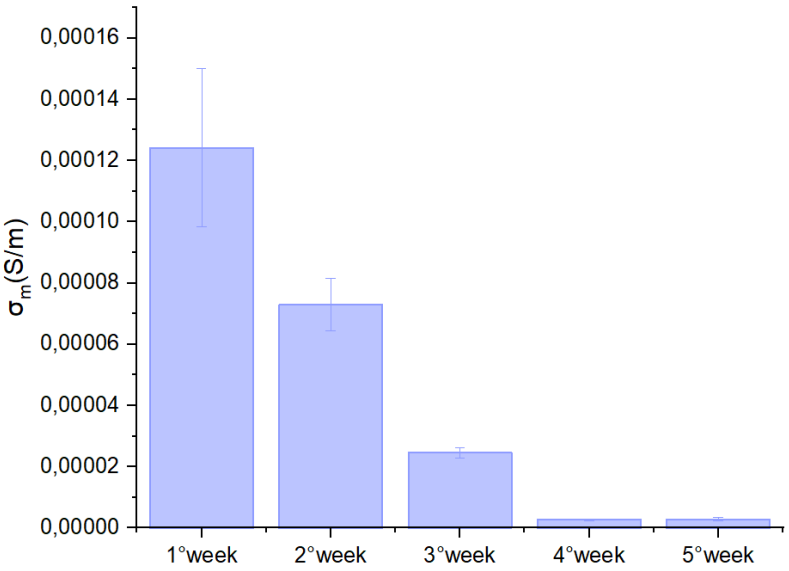

Figure 45 Statistical analysis of conductivity test results

The durability of the sample over time was assessed by looking at how the properties of the sample subjected to 50% deformation for 5 consecutive weeks varied.

From a mechanical point of view, from the stress-strain graph (*Fig. 46*) it is possible to see the trend of the curves over the weeks and it is possible to observe that at the fifth week, the sample begins to exhibit plastic behaviour.

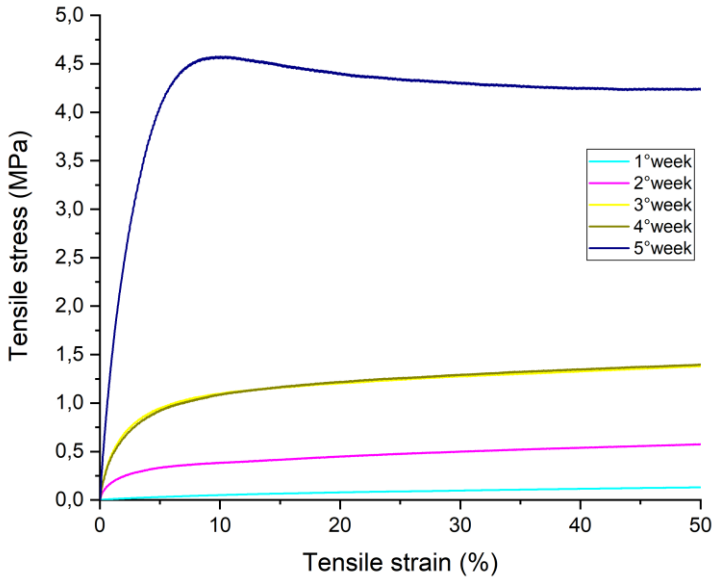

Figure 46 Stress-strain curve graph of durability tests carried out for 5 consecutive weeks.

This observation is also demonstrated in *Figure 47*, which represents the increase in elastic modulus over time, that after five weeks varies by almost two orders of magnitude and shows that the material has become more rigid.

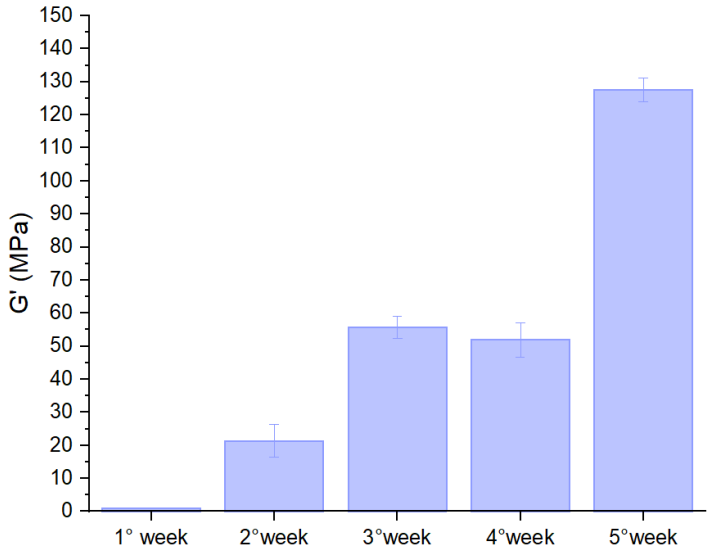

Figure 47 Variation of Young's Modulus over time after the sample has been subjected to 50% deformation for 5 consecutive weeks.

Also, for these tests, the samples were evaluated electrically and we see that unlike the mechanical test where it is clearly visible how the material becomes more rigid, in the electrical test, on the other hand, the sensitivity of the sample remains quite similar over time (*Fig. 48*).

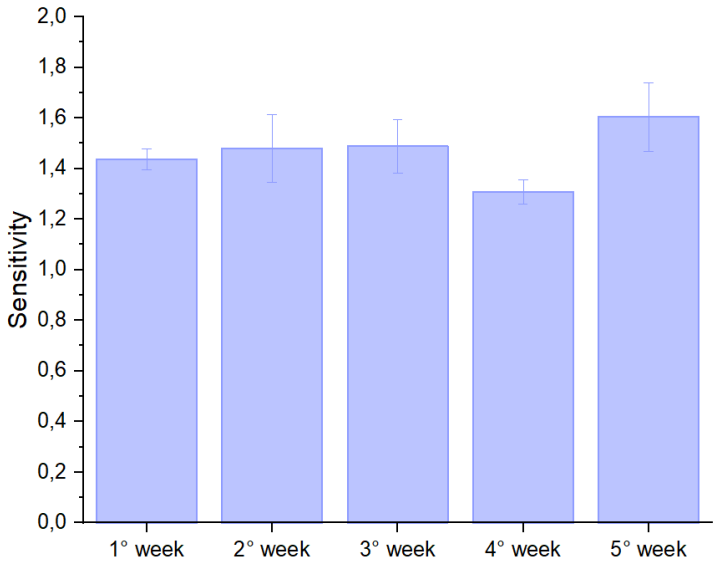

Figure 48 Variation in sample sensitivity when subjected to durability tests for 5 consecutive weeks.

In addition, in these durability tests, the sample was also tested as a force sensor and from the graph in *Figure 49* it is possible to see the strong variation in material properties over time, in particular at the fifth week the sample must feel a strong stress before detecting a change in electrical resistance.

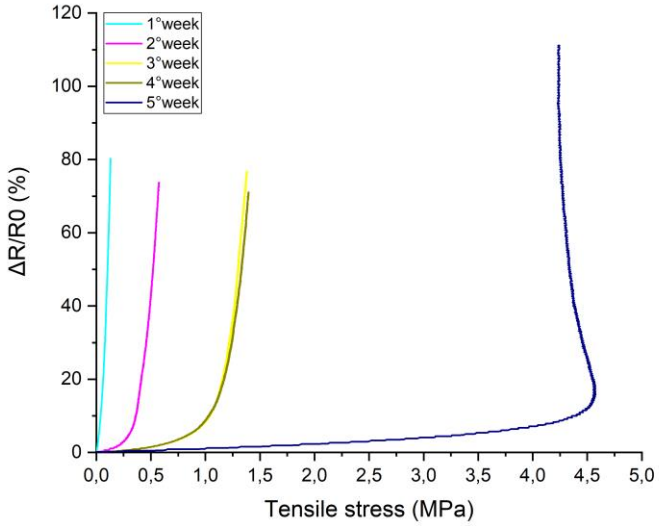

Figure 49 Results of the evaluation of the sample as a force sensor over time

4.5 Cytocompatibility tests

Finally, cytocompatibility tests were carried out to assess the use of the sensor in wearable applications.

Initially, the test was carried out in triplicate on samples containing 2wt% of PEGDA700 and 1.5wt% of TPO-SDS, from *Figure 50* it is possible to see the failure of the test as the percentage of surviving cells is very low. This result is mainly due to the presence of Sodium dodecyl sulphate (SDS) which is an anionic detergent that can be cytotoxic to cells as it can break down the cell membrane, denature proteins, over-stress cells and can also create mitochondrial dysfunction.

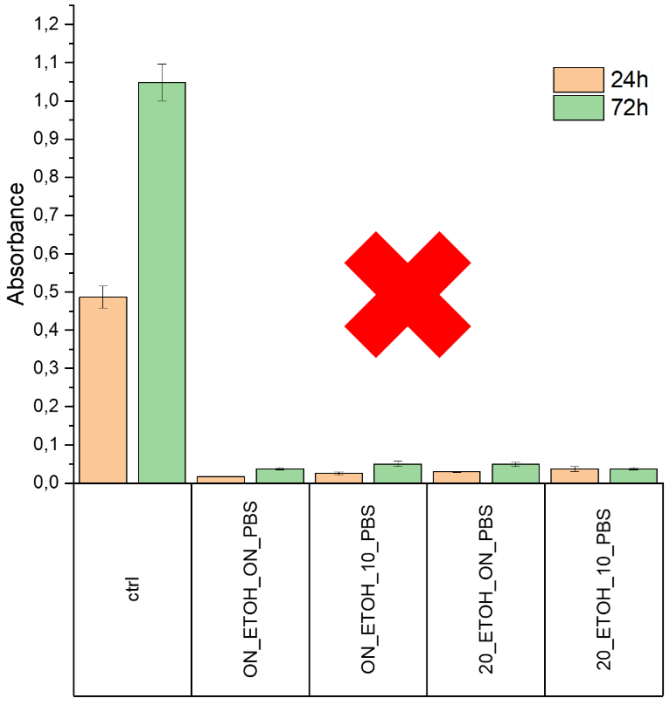

Figure 50 Results of the MTT metabolic assay on the sample containing the TPO-SDS

Afterwards, TPO-SDS was replaced with another photoinitiator, Lithium phenyl-2,4,6-trimethylbenzoylphosphinate (LAP), which is cytocompatible and give to the photocurable polymer similar mechanical properties to the previous one.

As shown in *Figure 51*, it can be seen that with the use of LAP, there is a general proliferation and growth of the cells for all types of washing, and consequently this determines the success of the experiment, which makes it possible to assert that the sample is not cytotoxic and therefore does not release substances harmful to the cells.

In particular, looking at the statistical analysis, it appears that the absorbance recorded for the washes:

- overnight in ethanol + overnight in PBS
- 20 minutes sonication in ethanol + overnight in PBS

is significantly different to the other washes, so from this observation it was possible to determine that the second one was the better wash as it stresses the cells less by having a shorter duration.

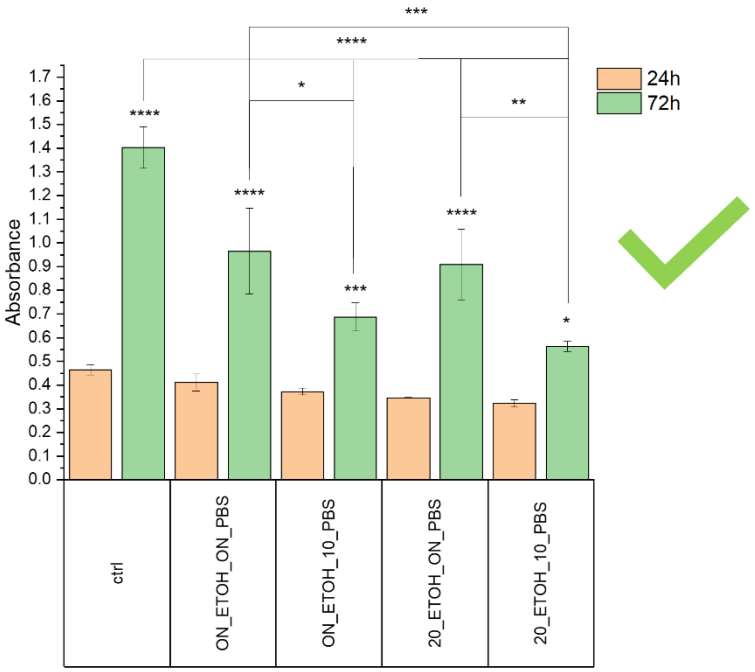

Figure 51 Results of the MTT metabolic assay on the sample containing LAP.

Chapter 5

Applications

Finally, the sensor was applied to the human body to verify its ability to detect a time-dependent variation in electrical resistance under different application conditions.

The sensor was applied to the finger in order to assess the change in electrical resistance over time as the bending angle of the finger changed. From the graph, it can be seen that the resistance can remain constant for a certain time while the finger is stationary in a specific position.

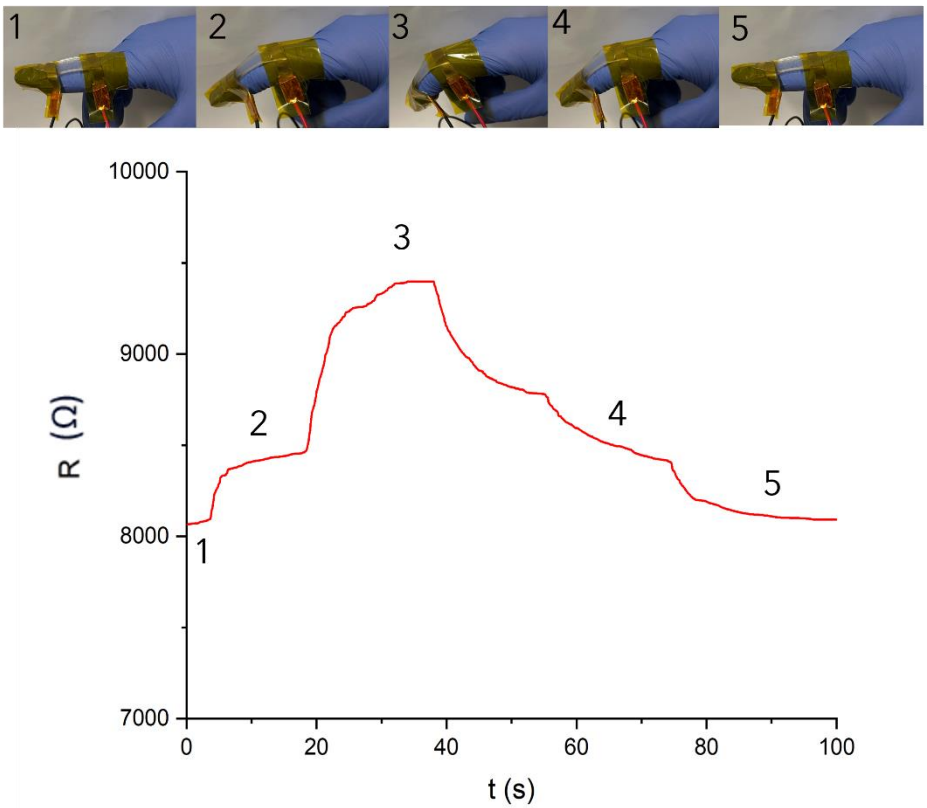

Figure 52 Finger bending tests at different angles.

In addition, the sensor was also used to evaluate different finger-bending frequencies as can be seen in the graph in *Figure 53*.

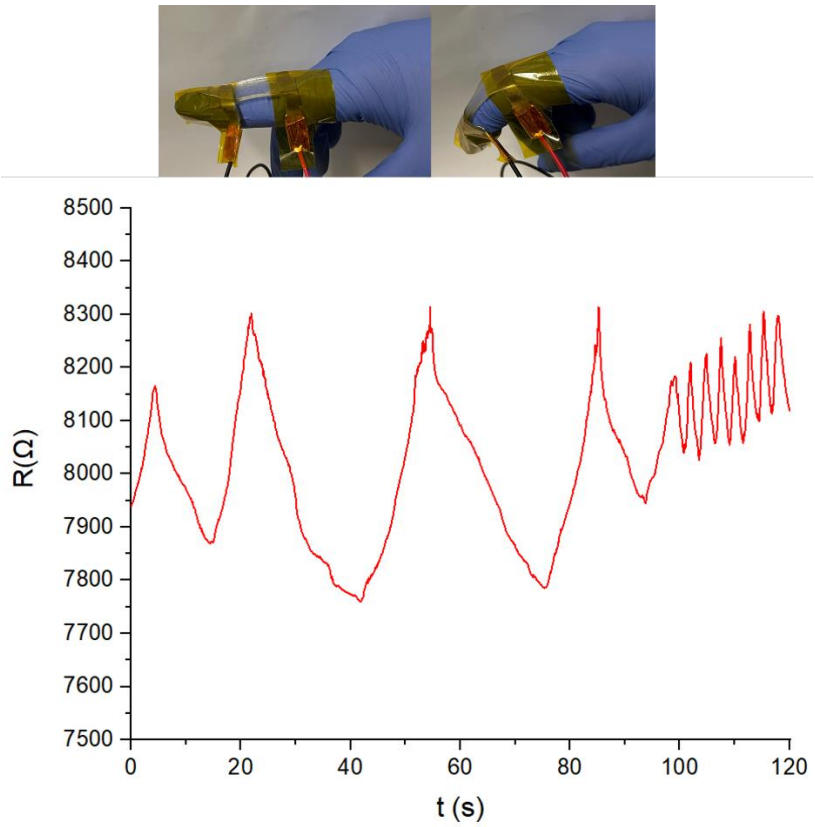

Figure 53 Finger bending tests at different frequencies.

Additionally, the sensor was placed on the forearm to assess its sensitivity in detecting small deformations by evaluating the movement of the finger flexor muscles during the opening and closing of the hand at different speeds (*Fig. 54*).

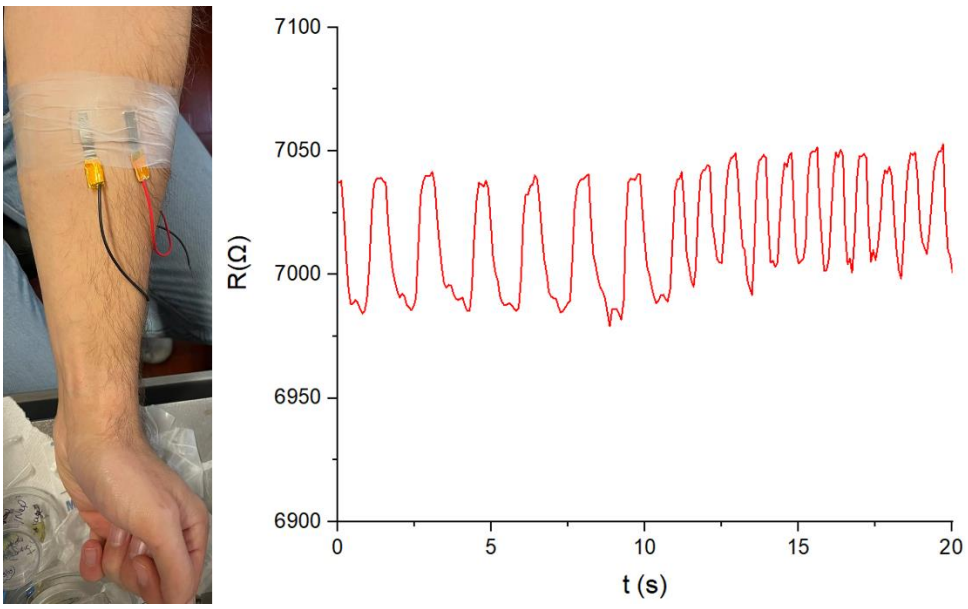

Figure 54 Test to check the sensor's ability to detect small deformations such as the movement of the hand flexor muscles.

Finally, the sensor was also applied on the throat to evaluate its ability to recognise a certain pattern; in fact, *Figure 55* shows the trend of electrical resistance over time due to the movement of the vocal cords during the pronunciation of the word 'CIAO'.

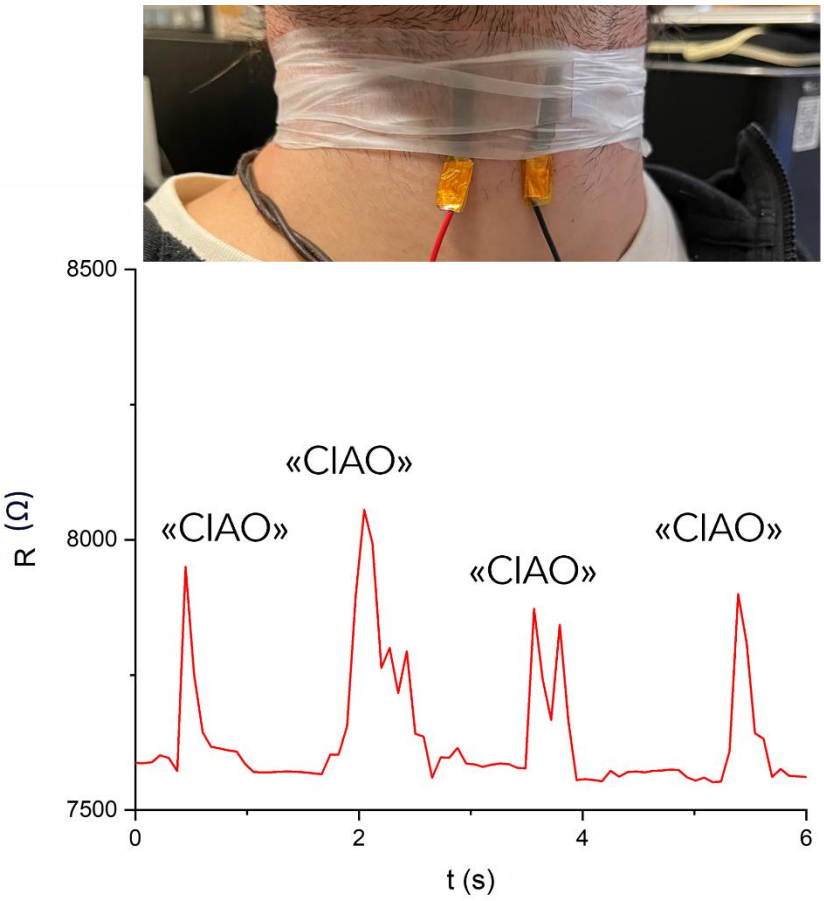

Figure 55 Test to verify the sensor's ability to recognise a certain patter such as that caused by the movement of the vocal cords when pronouncing the word 'CIAO'.

Chapter 6

Conclusions

In conclusion, a transparent, highly stretchable and conductive sensor was realised in this thesis work.

The sensor consists of ionic liquid which was added with 2wt% of PEGDA700, to form the 3D network, and 1.5wt% of TPO-SDS, to cross-link the formulation once exposed to UV light. In particular, two flat, thin stainless-steel electrodes were inserted during the crosslinking of the polymer to create a connection between the sensor and the instruments to measure the electrical properties.

The characteristic feature of this sensor is that the electrical conductivity is provided by the ionic liquid itself that forms the basis of the polymer matrix whose mechanical properties were improved by the presence of PEGDA700, which made the polymer less viscoelastic. Consequently, this allowed for a simple structure and an equally simple and fast manufacturing method.

In order to select at the formulation mentioned at the beginning of this section, the material underwent a series of characterisations at a chemical and electromechanical level. In particular, four formulations with different weight percentages of PEGDA700 were studied:

- LIa + 0wt% PEGDA700 + 1.5wt% TPO-SDS
- LIa + 1wt% PEGDA700 + 1.5wt% TPO-SDS
- LIa + 2wt% PEGDA700 + 1.5wt% TPO-SDS
- LIa + 5wt% PEGDA700 + 1.5wt% TPO-SDS

These characterisations showed that in general all formulations are very reactive, but the formulation containing 2wt% PEGDA700 was found to be a good compromise in terms of chemical and mechanical properties compared to the other formulations. In fact, from a mechanical point of view, it allowed a sample elongation of almost 300% before failure and a gauge factor of 1.75.

From the electrical point of view, on the other hand, it exhibited good stability during cyclic tensile tests, indicating a low viscoelastic behaviour of the material, which allows repeatable samples to be obtained.

Subsequently, other samples were made with the selected formulation and then subject to further characterisation at a chemical, electromechanical and finally biological level. In particular, at the chemical level, it was observed that the sample is well cross-linked as in the %GEL tests, the percentage of unreacted formulation is less than 10%. From an electro-mechanical point of view, its stability over time was evaluated. In particular, a strong variation was observed both at the level of electrical conduction where conductivity values, after five weeks, strongly decrease. In addition, a strong change in properties was also observed from a mechanical point of view, after five weeks, the sample becomes much stiffer with a Young modulus of around 130MPa, two orders of magnitude higher than the initial one. A positive aspect, however, is the sensitivity, which remains fairly constant over time with a gauge factor around 1.5.

Finally, biological characterisation gave negative results with complete cell death due to the presence of the photoinitiator TPO-SDS and more specifically Sodium dodecyl sulphate (SDS), which is a cytotoxic agent. Subsequently, it was replaced with the biocompatible photoinitiator Lithium phenyl-2,4,6-trimethylbenzoylphosphinate (LAP), which has similar mechanical properties to TPO-SDS. Thanks to this substitution, cytocompatibility tests were successful and good cell proliferation and growth was observed.

Finally, as a result of all these characterisation methods, the sample was also tested applied to the body and showed good performance in detecting different finger bending angles and also different bending frequencies. In addition, it was also able to detect small deformations such as the movement of the hand flexor muscles and the vibrational movement of the vocal cords following the pronunciation of the word 'CIAO'.

However, there are still many aspects to be improved, e.g. further work could be done on optimising the stability of the samples over time, or as it is

photocurable, the formulation could be optimised to also be used in 3D printing techniques.

In conclusion, the sensor realised is a good starting point to obtain in the future an electronic skin to be used on patients with severe skin damage or to integrate it in robotic prostheses to help patients who have undergone limb amputation.

Bibliography

[1] W. Wang *et al.*, 'Neuromorphic sensorimotor loop embodied by monolithically integrated, low-voltage, soft e-skin', *Science (1979)*, vol. 380, no. 6646, pp. 735–742, May 2023, doi: 10.1126/science.ade0086.

[2] P. A. J. Kolarsick, M. A. Kolarsick, and C. Goodwin, 'Anatomy and Physiology of the Skin', *J Dermatol Nurses Assoc*, vol. 3, no. 4, pp. 203–213, Jul. 2011, doi: 10.1097/JDN.0b013e3182274a98.

[3] C. P. Ryan, G. C. Bettelani, S. Ciotti, C. Parise, A. Moscatelli, and M. Bianchi, 'The interaction between motion and texture in the sense of touch', *Journal of Neurophysiology*, vol. 126, no. 4. American Physiological Society, pp. 1375–1390, Oct. 01, 2021. doi: 10.1152/jn.00583.2020.

[4] Q. T. Lai, Q. J. Sun, Z. Tang, X. G. Tang, and X. H. Zhao, 'Conjugated Polymer-Based Nanocomposites for Pressure Sensors', *Molecules*, vol. 28, no. 4. MDPI, Feb. 01, 2023. doi: 10.3390/molecules28041627.

[5] T. D. Nguyen and J. S. Lee, 'Recent development of flexible tactile sensors and their applications', *Sensors*, vol. 22, no. 1. MDPI, Jan. 01, 2022. doi: 10.3390/s22010050.

[6] C. Zhao *et al.*, 'Ionic Flexible Sensors: Mechanisms, Materials, Structures, and Applications', *Advanced Functional Materials*, vol. 32, no. 17. John Wiley and Sons Inc, Apr. 01, 2022. doi: 10.1002/adfm.202110417.

[7] S. Stassi, V. Cauda, G. Canavese, and C. F. Pirri, 'Flexible tactile sensing based on piezoresistive composites: A review', *Sensors (Switzerland)*, vol. 14, no. 3. MDPI AG, pp. 5296–5332, Mar. 14, 2014. doi: 10.3390/s140305296.

[8] T. Y. Kim, W. Suh, and U. Jeong, 'Approaches to deformable physical sensors: Electronic versus iontronic', *Materials Science and Engineering R: Reports*, vol. 146. Elsevier Ltd, Oct. 01, 2021. doi: 10.1016/j.mser.2021.100640.

[9] P. Zhao *et al.*, 'Strain-Discriminable Pressure/Proximity Sensing of Transparent Stretchable Electronic Skin Based on PEDOT:PSS/SWCNT Electrodes', *ACS Appl Mater Interfaces*, vol. 12, no. 49, pp. 55083–55093, Dec. 2020, doi: 10.1021/acsami.0c16546.

[10] J. Yang *et al.*, 'Ultrasoft Liquid Metal Elastomer Foams with Positive and Negative Piezopermittivity for Tactile Sensing', *Adv Funct Mater*, vol. 30, no. 36, Sep. 2020, doi: 10.1002/adfm.202002611.

[11] S. H. Cho *et al.*, 'Micropatterned Pyramidal Ionic Gels for Sensing Broad-Range Pressures with High Sensitivity', *ACS Appl Mater Interfaces*, vol. 9, no. 11, pp. 10128–10135, Mar. 2017, doi: 10.1021/acsami.7b00398.

[12] D. Ho, 'The Piezoionic Effect: Biomimetic Transduction Mechanism for Sensing, Actuation, Interface, and Energy Harvesting', *ChemElectroChem*. John Wiley and Sons Inc, 2023. doi: 10.1002/celc.202300268.

[13] K. Chen and D. Ho, 'Piezoionics: Mechanical-to-ionic transduction for sensing, biointerface, and energy harvesting', *Aggregate*. John Wiley and Sons Inc, 2023. doi: 10.1002/agt2.425.

[14] Y. Hu *et al.*, 'Ionic liquids revolutionizing biomedicine: recent advances and emerging opportunities', *Chemical Society Reviews*, vol. 52, no. 20. Royal Society of Chemistry, pp. 7262–7293, Sep. 26, 2023. doi: 10.1039/d3cs00510k.

[15] K. Mishra *et al.*, 'Ionic Liquid-Based Polymer Nanocomposites for Sensors, Energy, Biomedicine, and Environmental Applications: Roadmap to the Future', *Advanced Science*, vol. 9, no. 26. John Wiley and Sons Inc, Sep. 01, 2022. doi: 10.1002/advs.202202187.

[16] G. Choudhary *et al.*, 'Ionic liquids: environmentally sustainable materials for energy conversion and storage applications', *Environmental Science and Pollution Research*. Springer Science and Business Media Deutschland GmbH, 2023. doi: 10.1007/s11356-023-25468-w.

[17] S. Peng *et al.*, 'Tailoring of photocurable ionogel toward high resilience and low hysteresis 3D printed versatile porous flexible sensor', *Chemical Engineering Journal*, vol. 439, Jul. 2022, doi: 10.1016/j.cej.2022.135593.

[18] N. Jiang *et al.*, 'Flexible, transparent, and antibacterial ionogels toward highly sensitive strain and temperature sensors', *Chemical Engineering Journal*, vol. 424, Nov. 2021, doi: 10.1016/j.cej.2021.130418.

[19] S. F. Klimaschewski, J. Küpperbusch, A. Kunze, and M. Vehse, 'Material investigations on poly(ethylene glycol) diacrylate-based hydrogels for additive manufacturing considering different molecular weights', *Journal of Mechanical and Energy Engineering*, vol. 6, no. 1, pp. 33–42, Jul. 2022, doi: 10.30464/jmee.2022.6.1.33.

[20] A. A. Pawar *et al.*, 'High-performance 3D printing of hydrogels by water-dispersible photoinitiator nanoparticles', *Sci Adv*, vol. 2, no. 4, Apr. 2016, doi: 10.1126/sciadv.1501381.

[21] A. Chiappone, I. Roppolo, E. Scavino, G. Mogli, C. F. Pirri, and S. Stassi, 'Three-Dimensional Printing of Triboelectric Nanogenerators by Digital Light Processing Technique for Mechanical Energy Harvesting', *ACS Appl Mater Interfaces*, Nov. 2023, doi: 10.1021/acsami.3c13323.